Thèse

présentée à

l'Université de Provence

pour obtenir le grade de

docteur ès sciences physiques

par

Pierre Albarède

SELF-ORGANIZATION IN THE 3D WAKES OF BLUFF BODIES

tome 2: texte anglais

Soutenance le 3 juin 1991, devant le jury composé de MM.

Louis Boyer, directeur

Pierre Coullet

Yves Pomeau, président

Jean Pierre Rivet

Paul Clavin

Christian Mathis

Michel Provansal

David Tritton

Rapporteurs:

Yves Pomeau

Peter A. Monkewitz

		·	

Foreword

This report is divided into three volumes:

volume 1: French text

volume 2: English text

volume 3: figures

Address

Laboratoire de Recherche en Combustion
UA 1117 CNRS - Université de Provence
service 252 faculté de Saint Jérôme
13397 Marseille CEDEX 13
tel (33) 91 28 84 13; fax (33) 91 63 52 61

Contents

- 0. Symbols and abbreviations, definitions
- 1. Introduction
 - 1.1. Survey of experimental results and contradictions
 - 1.2. The nature of 3D effects at low Reynolds numbers
- 2. Building a model
 - 2.1. Weakly 3D flow
 - 2.2. The plane wake: useful remarks and proposal for a Landau model
 - 2.3. A Ginzburg-Landau model for the weakly 3D wake
- 3. The time-sinusoidal solution of the GLC0 model for a uniform flow (analytical and numerical results)
 - 3.1. Transformations and scaling
 - 3.2. Exact results
 - 3.3. Approximate results .
 - 3.4. The transient (starting from noise)
- 4. Experiments showing the time-sinusoidal solution of the GLC0 model
 - 4.1. Near threshold experiments
 - 4.2. Far from threshold experiments
- 5. Time quasi-periodic fluctuations
 - 5.1. The odd mode and end cells
 - 5.2. A theoretical explanation for Williamson's transition at $Re_w = 64$
- 6. Conclusion

Appendix:

- A1. Definition of the complex amplitude A
- A2. Streamwise description of the wake
- A3. Useful results: the Landau equation, the phase diffusion equation
- A4. Experimental arrangement and numerical method

References

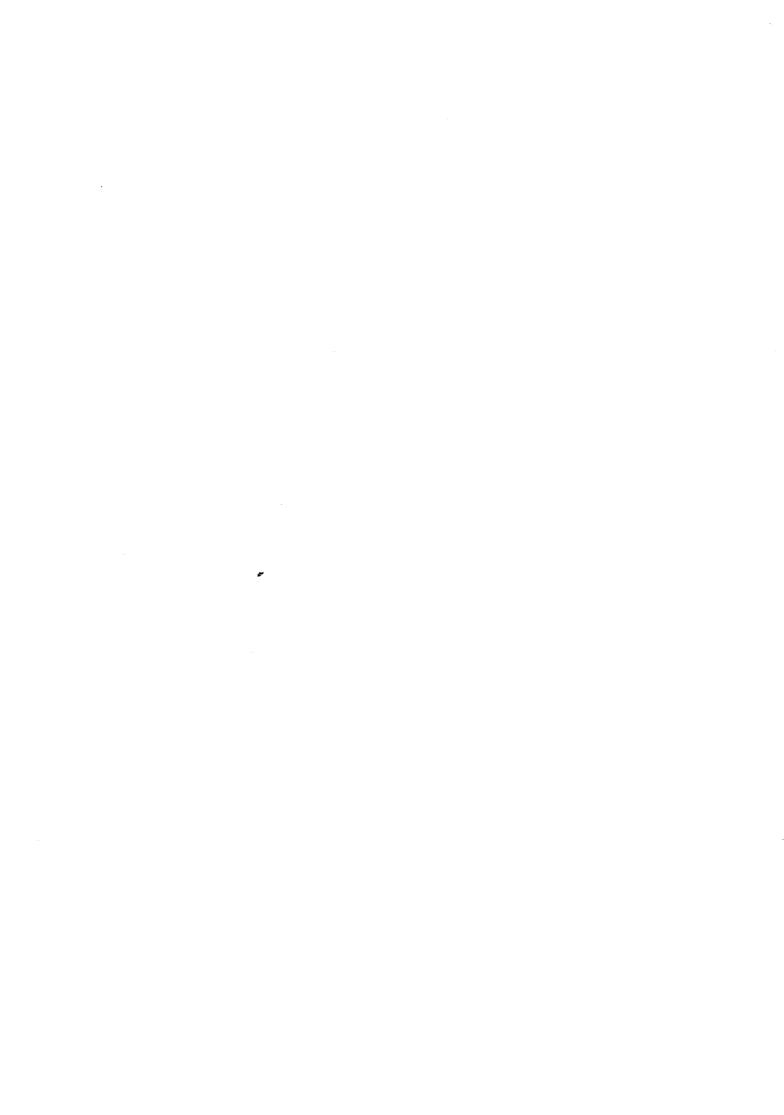
Bibliography

0. Symbols and abbreviations, definitions

Symbols and abbreviations	
free stream velocity	V_{∞}
obstacle diameter	
kinematic viscosity	ν
density (mass per unit volume)	
length of the obstacle	L
two-dimensional	2D
three-dimensional	3D
Reynolds number	Re
critical Re for the plane wake	Re ₀
critical Re for the 3D wake	
upper limit for the suppression of the odd mode	
upper limit for the existence of the broken chevron	
End Plate Boundary Layer	
Ginzburg-Landau equation	
with	
variable coefficients	. GLV
constant coefficients	
Kuramoto rescaling	GLK
no-oscillation boundary conditions	
periodic boundary conditions	
(and any combination of options, like GLCK0, GLV1)	
equality, in a definition	=
much greater (lower) than	» («)
approximately equal to	≈
equivalent to	. ~
For a complex number c:	
real partc _r	
imaginary partc _i	= imag(c)
complex conjugate	C*
argument (phase)	
the set of signed integers	
LASER Doppler Anemometry	LDA

Definitions

- Steady: time independent.
- The basic flow: the steady flow around the obstacle, stable below the critical Reynolds number.
- The bifurcating flow: the unsteady flow replacing the basic flow above the critical Reynolds number.
- z: coordinate along the obstacle axis.
- · Uniform: z-independent, within some interval.
- 2D: continuous translational invariance along z.
- 3D: the opposite of 2D.
- Plane wake: the flow around a disk in the plane (x, y) (a mathematical problem).
- For any real number r, int(r) is the highest signed integer lower than r.
- Energy: squared amplitude modulus |A|2



SELF-ORGANIZATION IN THE 3D WAKES OF BLUFF BODIES

The wake of elongated bluff bodies is considered as a field of interacting fluid oscillators, governed by a Ginzburg-Landau equation, with no-oscillation boundary conditions. In the case of a uniform basic flow, this dynamical reduction reproduces accurately most 3D features of the real wake at low Reynolds numbers.

1. Introduction

The wake of an obstacle is a 3D external open flow. "Open" means that the fluid domain is not bounded. In internal open flows, like the flow in a pipe, the fluid is surrounded by solid walls; here, on the contrary, solid walls are surrounded by the fluid. Moreover, I choose to observe the wake in the assumed inertial frame of the obstacle, focusing on the **near** wake. A model is provided for the wake of an **elongated**, **but finite**, obstacle: it consists of a Ginzburg-Landau equation (GL) and no-oscillation boundary conditions; some original mathematical features of the solutions are demonstrated, and compared with experiments.

I consider an elongated revolution body: the axis is labeled z, the length L is much greater than any diameter d(z), and the upstream flow is everywhere perpendicular to z, with a uniform direction x, and a steady magnitude $V_{\infty}(z)$ (c.f. DRA 01). Obstacle **vibrations are excluded**.

1.1. Survey of experimental results and contradictions

A reasonable idea is that the Navier-Stokes equations for wakes have steady solutions, with steady boundary conditions. However, because of hydrodynamical instability, wakes are often unsteady. Bluff bodies are likely to produce unstable wakes, at least because their blunt shapes strongly distort the flow.

The wake of a circular cylinder in a uniform upstream flow has been thoroughly studied for more than one century. When increasing the Reynolds number $\text{Re} = V_{\infty} \text{d/v}$ above a critical value close to 50, a t-periodic (periodic function of time t) fluctuation appears, leading to vortex shedding: this is the Bénard-von Kármán instability. In the 1950's, Tritton (ref. 1) noticed that in the

range 70 < Re < 90, the flow became t-quasi-periodic (time quasi-periodic). He attributed the second frequency to a different shedding regime of the plane wake. Lim (ref.), who found t-quasi-periodic instabilities of the (plane) von Kármán inviscid potential solution, recently referred to Tritton's hypothesis.

However, comparing Tritton's visualizations and velocity traces with work performed ever since (by, among others, Gaster (ref.), Gerrard (ref.)) leaves no doubt that he had a 3D wake, with spanwise cells oscillating at distinct frequencies and separated by vortex dislocations. In fact, even t-periodic wakes are hardly 2D: the vortex cores are not parallel to the z-axis. Berger (ref.) and Gerrard (ref.) reported oblique shedding, consisting in straight vortices, but not in the direction of the z-axis, while Hama (ref.), or Slaouti and Gerrard (ref.), observed parenthesis-shaped vortices. Sometimes, 3D vortices break, producing cells and t-quasi-periodic fluctuations. The explanation of these various 3D effects has motivated scores of papers for nearly thirty years.

Gaster (ref.) produced a second frequency and bent vortices by imposing a non-uniform basic flow. He proposed that a discontinuity in the frequency-velocity relation occurred when the node between two cells moved across the probe. Curiously, he could not get rid of a second frequency, even though the flow was apparently uniform (Gaster (ref. 2)).

Obstacle vibrations are quite a confusing effect, that Berger (réf.) addressed very soon, and cleverly applied to wake control. Berger and Wille (ref.) reviewed numerous contradictory experiments. Sreenivasan (ref.), seeking an example for some general features of transition to turbulence, observed windows of chaos in the wake of an obstacle. Van Atta and Gharib (ref.) revealed that aero-elastic coupling was involved in his observations. Their "measurements suggest that if there were absolutely no vibration a Strouhal-Reynolds number (frèquency-velocity) plot would have absolutely no discontinuities".

Slaouti and Gerrard (ref.) "found that the wake structure was strongly affected by the flow configuration near the **ends** of the body, which itself depended entirely on the constraints imposed by the end construction". More precisely, Gerich and Eckelmann (ref.) identified end cells in the following cases: either an end plate (with a boundary layer, denoted EPBL) or a free end (with a pressure short-circuit around the tip, increasing the base pressure). Williamson (ref. 2) showed that the end effect could even **propagate** from the end through the whole span, imposing oblique shedding and various 3D effects, without either flow non-uniformity or vibrations.

A theoretical advance occurred in the 1980's: the (global) stability properties of the plane wake were related to the (local) stability properties of the velocity

profiles at different x locations (Huerre and Monkewitz (ref.)). This approach had the physical qualities of locating the obstacle, thus allowing disturbances to grow in space (and time). As noticed by Monkewitz (ref. 1), the experiments and the modelization performed at L.R.C. - by my predecessors Boyer, Mathis, Provansalshow that the Bénard-von Kármán instability is an absolute instability: disturbances grow in place, leading to self-sustained oscillations (even if noise were turned off, oscillations would remain). The absolutely unstable velocity profiles are located in a finite area, the "wave maker", downstream from the obstacle. Even more strikingly, Triantafyllou and Karniadakis (ref.) affirmed: "the vortex wakes of bluff bodies can be reproduced by only knowing the time average flow at one specific location behind the object, where it is most unstable according to linear theory." In the Landau model developed at L.R.C., a single oscillator, i.e. a complex function of time A(t), stood for the wave maker. The time evolution equation for A was an autonomous equation, meaning that the wave maker, dictating its instability to the whole wake, evolved on its own. Quite remarkably, the same ideas had risen simultaneously from theory and experimental practice.

However, t-quasi-periodicity remained unexplained. The numerical simulations of the Navier-Stokes equations for the plane wake didn't show either any t-quasi-periodic fluctuation (Karniadakis and Triantafyllou (ref.), Sa and Chang (ref.)).

The results of Mathis, Provansal, Boyer (réf. 1) confirmed that t-quasiperiodicity implied 3D effects. Louis Boyer asked me to improve the Landau model, in order to explain those space-time effects.

1.2. The nature of 3D effects at low Reynolds numbers

At first sight, the basic flow of greatest theoretical interest is the 2D one. Unfortunately, not much information is available about this flow, because it does not exist in nature, and its numerical study is still a difficult task. However, at low Reynolds numbers, its instability is probably 2D (parallel shedding), for a theoretical reason: the Squire's theorem (Drazin and Reid (ref.)); and an experimental reason: stable parallel shedding can be obtained with a finite geometry by manipulating the end conditions (Eisenlohr and Eckelmann (ref.), Williamson (ref. 2), Hammache and Gharib (ref.)).

At higher Re, Hama (ref.), Provansal (ref.) and Williamson (ref. 1) observed z-periodic patterns, with a wave length independent of the aspect ratio L/d. This can be interpreted as a secondary instability of the 2D flow: in the simpler case,

the 2D bifurcating flow becomes linearly unstable with respect to some z-sinusoidal disturbance (z-sinusoidal because, in short, a linear differential equation with constant coefficients is involved). In reality, the sudden appearance of highly non-linear patterns, like horse-shoe vortices, and the existence of hysteresis, imply that finite amplitude perturbations are involved in the transition.

The present work does not deal with this kind of 3D instability: it is restricted to low Reynolds numbers, where **no 3D instability of the 2D basic flow exists** (Re < 180 resulting from Williamson (ref. 1)). So, why are there so many 3D effects at low Reynolds numbers? Among all possible reasons, one is just unavoidable: real flows are bounded along z, and, so far, this **finite length effect** has never been clearly recognized.

Near the threshold, the characteristic length scale is diverging, as expected from the bifurcation theory of spatially extended systems (Kuramoto (ref.)), and cannot be neglected before L, however great. As the instability cannot develop freely, a quasi-linear behaviour is obtained. Further above the threshold, through a highly non-linear saturation process, the pattern becomes roughly independent of L, and the finite length effect becomes the **end effect**.

The hypothesis of a uniform basic flow and a finite length proves capable of explaining many experimental 3D effects, that were formerly attributed to other causes, like flow non-uniformity. Actually, the confusion is easy, because most 3D effects have similar features (bent vortices, cells, vortex dislocations).

2. Building a model

2.1. Weakly 3D flow

Because of the obstacle elongation, the flow varies slowly along z. Thus, there may be some relation between the actual flow at some z, and the plane flow around the local cross-section, with the local upstream speed. This latter flow I call local wake.

The weakly 3D properties can be predicted by finding how all those local wakes live together; this is a self-organization problem, as defined by Haken (ref.) or Kuramoto (ref.). A diffusive coupling between local wakes is proposed as a lower order approximation of the actual coupling.

2.2. The plane wake: useful remarks and proposal for a Landau model

2.2.1. Dimensional analysis and the von Kármán model

All unknown quantities in the plane wake of a disk, are functions of the only four external parameters V_{∞} , d, v, p. The three independent units for Mass, Length and Time are M, L, T. As the problem is independent of the choice of units, any physical quantity x with unit M^a L^b T^c is linked to the external parameters by a non-dimensional function $x_{M,L,T}$ such as

$$\frac{x}{\mathcal{M}^{a} \mathcal{L}^{b} \mathcal{T}^{c}} = x_{\mathcal{M}, \mathcal{L}, \mathcal{T}} \left(\frac{V_{\infty}}{\mathcal{L}/\mathcal{T}}, \frac{d}{\mathcal{L}}, \frac{v}{\mathcal{L}^{2}/\mathcal{T}}, \frac{\rho}{\mathcal{M} \mathcal{L}^{3}} \right)$$

A canonical choice is L = d and $M = \rho d^3$. But there are three possibilities for T:

• Roshko time scale: $T = d^2/v$.

$$x/(\mathcal{M}^{a} \mathcal{L}^{b} \mathcal{T}^{c}) = x_{\mathcal{M}, \mathcal{L}, \mathcal{T}} (Re \equiv V_{\infty} d/v, 1, 1, 1) = x_{R} (Re)$$

$$\tag{1}$$

• Strouhal time scale: $T = d/V_{\infty}$.

$$x/(M^a L^b T^c) = x_{M,L,T} (1, 1, Re^{-1}, 1) = x_S (Re)$$
 (2)

• Lin time scale: $\tau = v/V_{\infty}^2$ (named after Berger and Wille (ref.), p.316)

$$x/(\mathcal{M}^a L^b \mathcal{T}^c) = x_{\mathcal{M}, L, \mathcal{T}} (Re^{-1}, 1, Re^{-2}, 1) = x_L(Re)$$
 (3)

The result of this dimensional analysis is that only one external parameter has to

be considered, the Reynolds number.

In the (2D) von Kármán model (c.f. DRA 02),

 κ the circulation of each vortex,

a the wave length, and

b the width of the vortex street

form a complete set of independent unknown quantities.

c, celerity of the vortex street (measured in the same frame as V_{∞}), is then given by

$$V_{\infty}$$
 - c = $\kappa/(2a)$ th(π b/a).

For the least unstable vortex street (Lamb (ref.)),

b/a = 0.281... and
$$V_{\infty}$$
 - c = $\kappa/(2\sqrt{2} a)$.

Two degrees of freedom cannot be determined because neither the viscous effects nor the obstacle are included.

Most features of the real wake depend on x. However, the frequency f does not, because the number of shed vortices is conserved. Precisely, if n(t, x) is the number of vortices per unit length along x,

$$\partial_{\uparrow} n + \partial_{\chi}(n c) = 0 \tag{4}$$

In experiments, n(t, x) is steady, and both terms in (4) are zero. The frequency f = n c does not depend on x. In 3D cases, when many cells are present, this property applies to each cell frequency. The t-quasi-periodic spectrum exhibits the same frequencies everywhere in the wake.

Thus, frequency is the quantity of easiest access in the problem. An experimental measurement of the plane wake frequency (though submitted to the interpretation of an actually 3D experiment) is Williamson's "universal curve" (Williamson (ref. 2), fig. 15). With the notation of (1), (2), (3), I keep the linear fit

$$f_R = fd^2/v \approx -5.1064 + 0.2175 \text{ Re} = Ro_0 + Ro_1 \text{ Re}$$
 Roshko number (5)

$$f_S = f_{P}/Re$$
 Strouhal number (6)

$$f_L = f_R/Re^2 = f_V/V_{\infty}^2$$
 Lin number (7)

At constant V_{∞} , one can check on (5) that d \rightarrow f is decreasing if and only if Re > -2 Ro₀/Ro₁ \approx 47.0 (8)

As the critical Reynolds number for the plane wake is $Re_0 \approx 49$ (estimates from § 4.1. range from 48.4 to 49.7), (8) is true, and even suggests that Re_0 be the critical point in the relation $d \rightarrow f$ at constant V_{∞} . Is this only a coincidence?

2.2.2. The Landau model

At first, I briefly recall some experimental results of Mathis, Provansal, Boyer (ref.): the loss of steadiness corresponds to the onset of an unstable mode. The fluctuating field is given by

$$v(Re, t, x = 5d, y = 0, z) = real(A(Re, t, z)),$$
 (1)

where A obeys a Landau equation

$$A_t = \sigma' A - I' |A|^2 A \tag{2}$$

with

$$\sigma' = \sigma_{r}' + i \sigma_{i}'; i' = i_{r}' + i i_{i}'.$$
 (3)

 σ_{r} ' depend on Re, and vanishes at Re = Re₁, the critical Reynolds number for the real wake, strongly depending on the aspect ratio. By convention, the linear pulsation σ_{i} '(Re) is positive. Saturation implies I_{r} ' > 0. But this model does not explain the following facts:

- Re₁, σ_i ' and Γ_i ' depend on the aspect ratio.
- The saturated energy (and Ir') depend on z (Mathis, Provansal, Boyer (ref. 2)).
- · A second mode appears when Re increases.

Clearly, these effects are 3D. I would rather have a model predicting them.

The first element of this model is a Landau model for the plane wake . The fluctuating field obeys

$$v(Re, t, x = 5d, y) = real(A(Re, t) f(y))$$
(4)

(an improved definition is given in appendix A1)

$$A_t = \sigma A - 1|A|^2 A \tag{5}$$

The t-sinusoidal asymptotic solution corresponds to the t-periodic asymptotic flow found in plane numerical simulations. σ and I are functions of the external parameters. (2.2.1.\$1) proves that $\sigma d^2/v$ and Iv are functions of Re only: $\sigma d^2/v = \sigma_R(Re)$ and, by definition of Re₀, $\sigma_{rR}(Re_0) = 0$.

It is now necessary to introduce the third space coordinate, z.

2.3. A Ginzburg-Landau model for the weakly 3D wake

The external parameters involved in (2.2.2.\$2) are Re(z) and d(z). The Landau model for the plane wake is applied to the local wake, and completed empirically with a diffusive coupling:

$$v(t, x = 5d(z), y, z) = real(A(t, z) f(y))$$
 (1)

$$\partial_{\uparrow} A = \sigma(\text{Re}(z), d(z)) A + \mu \partial_{z}^{2} A - I(\text{Re}(z)) |A|^{2} A$$
 (2)

The complex μ is, in general, a function of the basic flow, here the **functions** Re(z) and d(z).

The boundary conditions

A place where the fluid oscillation vanishes is called a **node**. If two nodes are located at z_1 and z_2 , then, following the method of § A4.2., (2) is solved on $[z_1, z_2]$ with the boundary conditions

$$A(t, z_1) = 0$$
 and $A(t, z_2) = 0$ (3)

As the obstacle length is finite, fluid oscillation must stop when $z \to \pm \infty$; therefore, two nodes, called external nodes, exist with a minimum and a maximum z. Experiments show that external nodes are located near the ends (z = \pm L/2). (3), applied at the external nodes, represents the physical boundary conditions. Confusing the locations of nodes and extremities,

$$A(t, \pm L/2) = 0 \tag{4}$$

The solution of (2) may produce nodes in the interior of the definition interval: these "internal" nodes have phase singularities, corresponding to vortex dislocations. Once the location of an internal node is known, it can be used as a boundary, without affecting the solution A(t, z). The solution on one side of the node is independent of the solution on the other side of the node: a node acts as a **screen**.

Other possible boundary conditions are periodic boundary conditions $A(t, -L/2) = A(t, L/2) \tag{5}$

They are not physically relevant (except for the wake of a torus!).

3. The time-sinusoidal solution of the GLC0 model for a uniform flow (analytical and numerical results)

3.1. Transformations and scaling

Transformations

If A(t, z) is a solution of the GL equation (2.3.\$2), then

- \bullet For any complex number u of modulus 1, u A(t, z) is still a solution (this property results in the marginal stability with respect to phase perturbations).
- For any real number ω , $exp(i\omega t)$ A(t,z) is a solution of

$$\partial_t A = (\sigma + i \omega)A + \mu \partial_z^2 A - I |A|^2 A$$
(1)

- A(-t, z)* is not a solution, unless the coefficients σ , μ , I are purely imaginary (case of a non-linear Schrödinger equation); however it is a solution of the conjugate equation; the signs of μ_i and l_i are relative to the convention adopted for the sign of σ_i .
- \bullet A(t, z) * is not a solution, unless the coefficients are real.
- A(t, -z) is a solution if the coefficients are even functions of z.

Kuramoto scales

In the 3D case, the length scale introduced in § 2.2.1. is $\mathbf{L} = d(z_0)$ where z_0 is the location of some typical local wake. Kuramoto proposes new scales, based on $\sigma_r(z_0)$, μ_r and $l_r(z_0)$:

$$A = A_{K} (\sigma_{r} / I_{r})^{1/2}, t = t_{K} \sigma_{r}^{-1}, z = z_{K} (\mu_{r} / \sigma_{r})^{1/2}$$
(2)

These new scales are always used in this chapter, and unnecessary indices K are dropped. For a uniform basic flow, the rescaled GL, or GLCK equation, is

$$A_{t} = (1+i c_{0}) A + (1+i c_{1}) A_{zz} - (1+i c_{2}) |A|^{2}A$$
with $c_{0} = \sigma_{i}/\sigma_{r}, c_{1} = \mu_{i}/\mu_{r}, c_{2} = I_{i}/I_{r}$. (3)

3.2. Exact results

The problem to solve is (3.1.\$3), with the boundary conditions:

$$A(\pm L_{K}/2) = 0 \tag{1}$$

The association of (3.1.\$3) and (1) is the problem GLCK0, indeed the main object of the present work. As c_0 affects the solution only by a frequency shift (from

(3.1.\$1)), the mathematical external parameters are c_1, c_2 and the **Kuramoto** length L_K , related to the physical external parameters Re and L_R by

$$L_{K} = L \sqrt{\frac{\sigma_{r}}{\mu_{r}}} = \frac{L}{d} \sqrt{\frac{\sigma_{r}d^{2}/\nu}{\mu_{r}/\nu}} = L_{R} \sqrt{\frac{\sigma_{rR}(Re)}{\mu_{rR}(Re)}}$$
 (2)

As long as the variation $(c_1, c_2)(Re)$ can be neglected, L_K alone represents the evolution of the wake when varying Re or L_R . As $\sigma_r(Re_0) = 0$,

$$L_K \to 0$$
 when Re \to Re₀ (3) (critical divergence of the Kuramoto length scale)

3.2.1. Analysis

Let a t-sinusoidal solution of GLCK0 be written

$$A(t, z) = R(z) \exp(i\phi(t, z)) \tag{1}$$

Useful notations are introduced:

$$\phi(t, z) = (c_0 - c_2)t + \Phi(t, z)$$

$$\omega = \Phi_{\mathsf{f}} \tag{2}$$

$$\Omega = \Phi_{\dagger} \tag{3}$$

$$q = \Phi_Z$$

 ϕ is the full phase; Φ is the shifted phase; the full pulsation ω is steady, by hypothesis; the shifted pulsation Ω vanishes for parallel shedding; q is the local wave-number. The boundary conditions are

$$R(\pm L/2) = 0$$
 and (by physical requirement) q bounded when $z \rightarrow \pm L/2$ (4)

The real and imaginary parts of GLCK reduce to

$$0 = R - R^3 + (R_{zz} - Rq^2) - c_1 (2R_z q + Rq_z)$$
 (5)

$$R \Omega = c_2(R - R^3) + c_1(R_{zz} - Rq^2) + (2R_z q + Rq_z)$$
(6)

After two independent linear combinations,

$$R\Omega = -(c_1 - c_2)(R - R^3) + (1 + c_1^2)(2R_z q + Rq_z)$$
(7)

$$c_1 R \Omega = (1 + c_1 c_2)(R - R^3) + (1 + c_1^2)(R_{zz} - Rq^2)$$
 (8)

Noticing

$$R(2R_zq + Rq_z) = (qR^2)_z \tag{9}$$

and using the boundary conditions (4), equation (7) leads to

$$\Omega(R) = -(c_1 - c_2) (1 - M_4(R, L/2) / M_2(R, L/2))$$
 (10)

$$q(R, z) = R^{-2}(z) \frac{C_1 - C_2}{1 + C_1^2} M_4(R, L/2) \left(\frac{M_2(R, z)}{M_2(R, L/2)} - \frac{M_4(R, z)}{M_4(R, L/2)} \right)$$
(11)

with the functional expression

$$M_n(R, z) \equiv \int_{-L/2}^{z} R(z')^n dz'$$
 (12)

Introducing R(z) = R_Z(0) Z + O(Z²) with Z = z+L/2 \rightarrow 0 in (11) leads to

$$q(R, z) = \frac{1}{3} \frac{c_1 - c_2}{1 + c_1^2} \frac{M_4(R, L/2)}{M_2(R, L/2)} Z + O(Z^2)$$
(13)

It is possible to eliminate q from (8) and (11). The resulting equation is

$$R_{ZZ} = -\partial_{R}E_{D}(\Omega, R(z)) + f(R, z)$$
(14)

where

$$E_p(\Omega, R) = u(\Omega) R^2/2 - v R^4/4$$
 (15)

$$u(\Omega) = (1 + c_1 c_2 - c_1 \Omega)/(1 + c_1^2), v = (1 + c_1 c_2)/(1 + c_1^2)$$
(16)

(u depends on R through Ω)

$$f(R, z) = R(z)^{-3} \left[\frac{c_1 - c_2}{1 + c_1^2} M_4(R, L/2) \left(\frac{M_2(R, z)}{M_2(R, L/2)} - \frac{M_4(R, z)}{M_4(R, L/2)} \right) \right]^2$$
(17)

(14) is the **equation of motion** for a pseudo-particle, with position R at pseudo-time z, submitted to the potential E_p and the non-conservative force f, depending on the history of motion and Ω . The energy is

$$E(z) = (1/2) R_z^2 + E_p(\Omega, R(z))$$
 (18)

It is not a constant of motion, since its pseudo-time derivative is the power of f:

$$\mathsf{E}_{\mathsf{Z}}(\mathsf{z}) = \mathsf{R}_{\mathsf{Z}}(\mathsf{z}) f(\mathsf{R}, \mathsf{z}) \tag{19}$$

By drawing the shape of the potential and checking whether a solution with R = 0 at two distinct z is possible, the following proposition follows:

if
$$v \ge 0$$
, then $u(\Omega) > 0$ (20)

(If $u \le 0$ and $v \ge 0$, the particle dropped at R = 0 never comes back, and there is no solution of (4), (5), (6).)

If $(q(z), R(z), \Omega)$ is a solution of (4), (5), (6), then $(-q(-z), R(-z), \Omega)$ is also a solution; this can be checked directly, but I give a proof on (10), (11), (14) as a test of coherence. I define, for any function f, the function Tf by

$$Tf(z) \equiv f(-z) \tag{21}$$

I get successively

$$M_n(TR, z) = M_n(R, L/2) - M_n(R, -z)$$
 (22)

q(TR, z) = -Tq(R, z)

$$Tf(R, z) = f(TR, z)$$
 (23)

 $\Omega(TR) = \Omega(R)$

$$\partial^2_{zz}\operatorname{TR}(z) = \operatorname{T}\partial^2_{zz}\operatorname{R} = -\partial_{\mathsf{R}}\operatorname{E}_{\mathsf{p}}(\Omega(\operatorname{TR}),\operatorname{TR}(z)) + f(\operatorname{TR},z)$$

 $(-Tq, TR, \Omega)$ is a solution of (10), (11), (14).

The problem of unicity and existence of a t-sinusoidal solution for the GLCK0 model has been reduced as follows: find (R,Ω) such as

- $R(\pm L/2) = 0$.
- Ω is a function of R given by (10).
- R(z) is the motion of a particle submitted to a potential and a non conservative force depending on R(z') (z' < z) and Ω .

I now admit that this problem has no more than one solution (here, as in many other cases, unicity results from non-linearity). An immediate consequence is Tq = -q and TR = R (24)

3.2.2. How to build a solution

If Ω were known, (3.2.1.\$14) would be causal, and could be integrated as any other mechanical equation of motion, the particle being launched from the position R = 0 at time z = -L/2, with some given speed R_z(-L/2). This gives the idea of determining Ω and R by alternate successive approximations. The recurrence is initiated by Ω = 0 (parallel shedding shifted pulsation), and iterated as follows.

For some given Ω , I look for an initial velocity R_Z such as the particle left at R = 0 with velocity R_Z comes back after the pseudo-duration L (or, using the parity of R, makes U-turn after the pseudo-duration L/2). This is a corrected shoot method. The motion is actually a half (or a quarter) period of a periodic motion. f vanishes at z = p L/2, $p \in Z$, and does not hamper the qualitative study of motion.

The existence of a solution depends on the value of L and the signs of u and v. The case u > 0, v > 0 is treated on DRA 03, with the qualitative shapes of $E_p(R)$ and R(z) for various initial values of R_z . The z-period is greater than the linear period π and all values L > π lead to a unique solution. When L $\rightarrow \infty$, the particle makes U-turn closer and closer to the maximum of E_p :

$$\lim_{L \to \infty} R(0)^2 = \frac{u}{V} = 1 - \frac{c_1 \Omega}{1 + c_1 c_2}$$
 (1)

Once R has been obtained, a hopefully better value of Ω can be deduced from (3.2.1.\$10) and used to compute, if possible, a better R, and so on. The convergence towards a solution is likely. However, I leave the proof to somebody else, and I admit the **existence** of a t-sinusoidal solution for GLCK0.

Of course, the stability of the solution is still an other problem, treated numerically in § 5.2.. But I give the idea of an analytical approach, in the case u > 0, v > 0 (c.f. DRA 03). The particle oscillates in the crater of the "volcano-shaped" potential E_p ; if it skims the "crater rim" at pseudo-time z = 0, the z-period L_K tends to infinity; then, a finite amplitude perturbation at z = 0 can drive it out of the crater, with no hope of return. Numerical transients indicate that such a perturbation actually occurs during the collision of phase shocks (near z = 0), prior to the setup of the asymptotic pattern (c.f. § 3.4.).

3.2.3. Particular case $c_1 = c_2$

In this case, GLCK is non-dispersive, since all plane waves have the same pulsation (c.f. (3.3.2.\$2)). It is easily shown that GLCKO has then a unique solution.

(3.2.1.\$10) and (3.2.1.\$11) give $\Omega = 0$ and q = 0; R is solution of

$$R_{zz} = -\partial_R E_p \text{ where } E_p(R) = R^2/2 - R^4/4$$
 (1)

After a first integration:

$$R_z^2/2 + E_p(R) = E_p(R(0))$$
 (2)

A second integration, using the boundary conditions, leads to a unique solution R(z), obeying

$$L = \Lambda(R(0))$$
 (3)

where

$$\Lambda(r) \equiv 2 \int_{0}^{1} \frac{dx}{\sqrt{(1-x^{2})\left[1-\frac{1}{2}r^{2}(1+x^{2})\right]}}$$
(4)

The function Λ can be expanded in powers of r^2 with a radius of convergence 1:

$$\Lambda(r)/\pi = a_0 + a_1 r^2 + a_2 r^4 + a_3 r^6 + a_4 r^8 + \dots$$
 (5)

$$a_0 = 1$$
; $a_1 = 3/8$; $a_2 = 57/256$; $a_3 = 0.15381...$; $a_4 = 0.11576...$ (6)

The saturation of R(0) with increasing L appears on NUM 01.

3.3. Approximate results

3.3.1. Near threshold approximations: few unstable linear modes

In a finite medium, with the boundary conditions (3.2.\$1), I diagonalize the operator $(1+ic_0) + (1+ic_1)\partial_7^2$. The eigenvalues are

$$\sigma_n = 1 - q_n^2 + i (c_0 - q_n^2 c_1)$$
 where $q_n = n \pi / L$, $n = 1, 2, ...$ (1)

The eigenfunction associated with σ_n is

$$S_{n}(z) = \sin(q_{n}(z+L/2)) \tag{2}$$

The general solution of the linearized problem

$$\partial_t A = (1 + i c_0) A + (1 + i c_1) \partial_z^2 A$$
 (3)

is consequently

$$A(t, z) = \sum_{n=1, 2, ...} A_n(t) S_n(z)$$
 (4)

 A_n is called "global complex amplitude" of mode (S_n, σ_n) and obeys

$$d_t A_n = \sigma_n A_n \tag{5}$$

$$A_{n}(t) = \exp(\sigma_{n}t) A_{n}(0)$$
 (6)

Mode (S_n, σ_n) is linearly unstable for L > n π . This proposition was proven in the particular case $c_1 = c_2$, n = 1, by $\Lambda(0) = \pi$ (§ 3.2.3.).

The solution of GLCK0 is still in the space of linear combinations (4), because it is stable under the operation $A \rightarrow |A|^2 A$. But **non-linear interaction** terms must be added to equations (5).

If 1< L/π < 2, all the modes but (S₁, σ_1) are linearly damped, and are eliminated "adiabatically":

$$A(t, z) = A_1(t) S_1(z)$$
 (7)

Plugging (7) into the GLCK equation (3.1.\$3), and neglecting components other than S₁, leads to a Landau equation on the global complex amplitude A₁:

$$d_t A_1 = \sigma_1 A_1 - (3/4) (1 + ic_2) |A_1|^2 A_1$$
(8)

The coefficient 3/4 originates from the relation $4 \sin^3(x) = 3 \sin(x) - \sin(3x)$. The asymptotic solution of (8) is

$$A_1 = R_1 \exp(i\omega_1 t) \tag{9}$$

with

$$R_1^2 = (4/3)(1 - q_1^2) \tag{10}$$

$$\omega_1 = c_0 - c_2 - q_1^2(c_1 - c_2); q_1 = \pi/L$$
 (11)

 $A(t, z) = A_1(t) S_1(z)$ is the sum of two plane waves with wave numbers $\pm q_1$ and pulsation ω_1 , interfering so as to obey the boundary conditions. The relation (10) confirms the coefficient a_1 given by (3.2.3.\$6).

If $2 < L/\pi < 3$, the modes with n > 2 are linearly damped, and I keep

$$A(t, z) = A_1(t) S_1(z) + A_2(t) S_2(z)$$
(12)

This leads to the coupled equations

$$d_t A_1 = \sigma_1 A_1 - (1 + ic_2) [(3/4)|A_1|^2 A_1 + (1/2) A_1^* A_2^2 + A_1 |A_2|^2]$$
(13)

$$d_t A_2 = \sigma_2 A_2 - (1 + ic_2) [(3/4)|A_2|^2 A_2 + (1/2) A_2^* A_1^2 + A_2|A_1|^2]$$
(14)

 A_1 can be calculated by neglecting A_2 in (13) (the resulting equation is (8)), and introduced in (14) as an external forcing. This leads to $\lim_{t\to\infty}A_2=0$. The unique t-sinusoidal solution $(A_1,A_2)=(R_1\exp(i\omega_1t),0)$ is also the asymptotic solution. Mode (S_2,σ_2) is **non-linearly damped** (forced to zero) by mode (S_1,σ_1) .

This can be generalized for any value of L: the GLCK0 model has a t-sinusoidal solution, that is in fact, with $R_n \geq 0$ and ϕ_n real,

$$A(t, z) = \exp(i\omega t) \sum_{1 \le n\pi \le L} R_n \exp(i\varphi_n) S_n(z)$$
(15)

Using (3.2.1.\$24), R_n with even n vanish: the modes (S_n, σ_n) with even n are non-linearly damped. The modes (S_n, σ_n) with odd n are present, but **entrained**. The solution may not have a uniform phase, corresponding to non parallel vortex shedding.

Something is wrong in the last approach: because of non-linear effects, the sum (15) must be extended to all n. For example, even if $1 < L/\pi < 3$, the modes $(S_n, \, \sigma_n)$ with $n=3,\, 5,\, \ldots$ are present because of non-linear coupling. This is taken into account in a calculation performed by Monkewitz (ref. 2), near $L=\pi$. A small $\epsilon>0$ is defined by

$$L \equiv \pi \ (1 + \varepsilon^2) \tag{16}$$

Convenient independent linear combinations of the real and imaginary parts of

GLCK are:

$$0 = R - R^3 + (R_{zz} - R\Phi_z^2) - c_1(2R_z\Phi_z + R\Phi_{zz})$$
(17)

$$R\Phi_{t} = (c_{1}-c_{2}) (R_{zz}-R\Phi_{z}^{2}) + (1+c_{1}c_{2}) (2R_{z}\Phi_{z}+R\Phi_{zz})$$
(18)

Definitions:

for
$$n \in \mathbb{Z}$$
, $f_n \equiv \cos(n \pi z/L)$, $g_n \equiv \sin(n \pi z/L)$; (19)

for odd n = 2k+1, $f_n = \cos(n \pi z/L) = (-1)^k S_n(z)$.

The t-sinusoidal solution is expanded in powers of ϵ :

$$q = \epsilon^{2} \phi_{22} g_{2} + \epsilon^{4} (\phi_{42} g_{2} + \phi_{44} g_{4}) + O(\epsilon^{6})$$
 (20)

$$R = \epsilon \rho_{11} f_1 + \epsilon^3 (\rho_{31} f_{1+} \rho_{33} f_3) + \epsilon^5 (\rho_{51} f_{1+} \rho_{53} f_{3+} \rho_{55} f_5) + O(\epsilon^7)$$
 (21)

$$\Omega = \Omega_0 + \varepsilon^2 \Omega_2 + \varepsilon^4 \Omega_4 + O(\varepsilon^6) \tag{22}$$

Plugging (20), (21), (22) into (17), (18) leads to:

• At order ε,

$$\Omega_0 = -\left(c_1 - c_2\right) \tag{23}$$

• At order ε^3 ,

$$0.11^2 = 8/3$$
 (24)

$$\rho_{33}/\rho_{11} = -(1+c_1c_2)/(12(1+c_1^2)) \tag{25}$$

$$\phi_{22} = -(c_1 - c_2)/(3(1 + c_1^2)) \tag{26}$$

$$\Omega_2 = 2(c_1 - c_2) \tag{27}$$

• At order ε^5 .

$$\rho_{31}/\rho_{11} = -3/4 + (1+c_1c_2)/(24(1+c_1^2)) + c_2(c_1-c_2)/(72(1+c_1^2))$$

$$\rho_{31}/\rho_{11} = -\frac{50 c_1^2 + (2c_1 - c_2)^2 + 51}{72 (1 + c_1^2)}$$
(28)

$$\Omega_4 = -\left(3 + \frac{1 + c_2^2}{18(1 + c_1^2)}\right) (c_1 - c_2)$$
 (29)

The remaining coefficients can also be calculated except ρ_{51} , that is left undetermined (because the system is not finite-dimensional). Setting c_1 - c_2 to zero in the expressions of ρ_{11} , ρ_{31} , ρ_{33} given by (24), (28), and (25) confirms a_2 given by (3.2.3.\$6).

What is new, compared with the Landau model (3.3.1.\$8)?

- About R: the negative sign of ρ_{33}/ρ_{11} shows that the sinusoidal shape of R is flattening near z=0 when increasing ϵ .
- About the full pulsation ω, now accounting for all the modes:

$$\omega = c_0 - c_1 + \varepsilon^2 2(c_1 - c_2) - \varepsilon^4 \left(3 + \frac{1 + c_2^2}{18(1 + c_1^2)} \right) (c_1 - c_2) + O(\varepsilon^6)$$
(30)

Comparing ω with ω_1 given by (11) leads to

$$\omega = \omega_1 - \varepsilon^4 [(1 + c_2^2) / (18(1 + c_1^2))] (c_1 - c_2) + O(\varepsilon^6)$$
(31)

In experiments, vortices are shed with a non-zero celerity; consequently, ω cannot vanish. By convention (§ 2.2.2.), $c_0>0$; accordingly, $\omega>0$, $\omega_1>0$, and, using (11), $c_0\text{-}c_1>0$. At given Re and LR, parallel shedding has the highest possible frequency: (31) imposes $c_1\text{-}c_2>0$. In summary, I keep as a hypothesis drawn from experiments

$$c_0 > c_1 > c_2$$
 (32)

• About q: as c_1 - $c_2 > 0$, $\phi_{22} < 0$, meaning that Φ or ϕ are decreasing from the center to the sides of the definition interval (at some given t). Since ϕ is also an increasing function of t ($\omega > 0$), the sides, with a lower phase, are late compared with the center. This corresponds to vortices bowing towards the obstacle ends.

3.3.2. Far from threshold solution

The plane wave solutions are, in an infinite medium:

$$A_q(t, z) = (1-q^2)^{1/2} \exp(i \omega_q t + i qz) \text{ with } |q| < 1$$
 (1)

$$\omega_{q} = c_{0} - c_{2} - q^{2} (c_{1} - c_{2})$$
 (2)

A₀, called parallel plane wave, corresponds to parallel shedding.

 $A_{q\neq 0}$, called oblique plane wave, corresponds to oblique shedding.

I refer to the restriction of a plane wave to some interval as a "plane wave **section**". (2) looks like (3.3.1.\$11), where q_1 would have been replaced by q. In experiments, the oblique shedding pulsation ($q \neq 0$) is lower than the parallel shedding pulsation (but still positive), confirming (3.3.1.\$32). This property is called **non-linear dispersion**.

There is now a question arising: what is the solution of the boundary condition problem GLCK0 when L is very large? Plane waves are expected to

emerge. Not so obvious is that the parallel plane wave, with pulsation $\omega_0 = c_0 - c_2$, is not recovered, because it doesn't fit the boundary conditions.

A first step is to solve the semi-infinite boundary condition problem:

$$R(t,0) = 0 \tag{3}$$

$$R_Z \rightarrow 0$$
 and $q_Z \rightarrow 0$ for all t, when $z \rightarrow \infty$ (4)

or, identically, A(t, z) far from the end is a plane wave section. Noticing that an analytical solution exists in the particular case $c_1 = c_2$, Clavin (ref.) proposed to expand the unknown (q(z), R(z), Ω) in powers of $\varepsilon = c_1 - c_2$:

$$q(z) = q_0(z) + \varepsilon q_1(z) + \varepsilon^2 q_2(z) + O(\varepsilon^3)$$
 (5)

$$R(z) = R_0(z) + \varepsilon R_1(z) + \varepsilon^2 R_2(z) + O(\varepsilon^3)$$
 (6)

$$\Omega = \Omega_0 + \varepsilon \Omega_1 + \varepsilon^2 \Omega_2 + O(\varepsilon^3)$$
 (7)

$$c_2 = c_1 - \varepsilon \tag{8}$$

Convenient combinations of (3.2.1.\$5) and (3.2.1.\$6) are (3.2.1.\$7) and (3.2.1.\$8). The results, found with the help of Provansal, are:

• At order 0:

$$\Omega_0 = 0 \tag{9}$$

$$R_{0zz} + R_0 - R_0^3 = 0 ag{10}$$

$$R_0 = th(z/\sqrt{2}) \tag{11}$$

· At order 1:

$$\Omega_1 = 0 \tag{12}$$

$$R_0^2(1-R_0^2) = (1+c_1^2)(q_1R_0^2)_z$$

$$q_1 = (\sqrt{2/3}) (1/(1+c_1^2)) R_0$$
 (13)

$$R_{1zz} + (1-3R_0^2)R_1 = (c_1/(1+c_1^2))(R_0-R_0^3)$$

$$R_1 = -(1/2\sqrt{2}) (c_1/(1+c_1^2)) z (1-R_0^2)$$
(14)

· At order 2:

$$\Omega_2 = 0 \tag{15}$$

$$(1+c_1{}^2)(q_2R_0{}^2+2q_1R_0R_1)_z=2R_0R_1(1-2R_0{}^2)$$

$$q_2 = (1/(3\sqrt{2})) (c_1/(1+c_1^2)^2)(-(\sqrt{2}/2) z (1-R_0^2) + R_0)$$
(16)

$$R_{2zz} + (1-3R_0^2) R_2 = (c_1/(1+c_1^2)) (1-3R_0^2) R_1 + q_1^2 R_0 + 3R_0 R_1^2$$

For $z \to \infty$, as expected, the solution is asymptotically a plane wave section,

meaning $q \to q_{\infty}$ and $R \to R_{\infty}$, with

$$q_{\infty} = \frac{\sqrt{2}}{3} \frac{1}{1 + c_1^2} (c_1 - c_2) + \frac{1}{3\sqrt{2}} \frac{c_1}{(1 + c_1^2)^2} (c_1 - c_2)^2 + O((c_1 - c_2)^3)$$
(17)

$$q_{\infty}^2 + R_{\infty}^2 = 1$$
 (18)

This plane wave section is not necessarily stable. The exact value of the shifted pulsation is

$$\Omega = -q_{\infty}^{2} (c_1 - c_2) = O(\varepsilon^3)$$
(19)

The full pulsation is

$$\omega = c_0 - c_2 + \Omega = c_0 - c_2 - q_{\infty}^2 (c_1 - c_2)$$
(20)

 q_{∞} is imposed by the boundary condition at z=0, although it is observable far from the end only. The effect of a single end is thus oblique shedding.

The case of a large, but finite length L is solved by numerical simulation.

3.3.3. A numerical example with $c_1 \neq c_2$ and a variable L

A series of computations (NUM 02, NUM 03, NUM 04, NUM 05, NUM 06, NUM 07) allows to check the ideas and formulas of § 3.3.1. and § 3.3.2..

When L is high, the situation near each end is identical to that of the semi-infinite case. Two oblique waves with opposite wave numbers connect at midspan (z = 0), through a phase diffusion process (c.f. § A3.2.). With $\varepsilon = q_{\infty}^2$, a = 0, b = 1, (A3.2.\$11) leads to

$$q(z) \sim -q_{\infty} th([(c_1-c_2)/(1+c_1c_2)] q_{\infty} z)$$
 (1)

$$R(z) = 1 - \frac{q_{\infty}^2}{2} \left(1 - \frac{1 + c_1^2}{1 + c_1 c_2} ch^{-2} \left(\frac{c_1 - c_2}{1 + c_1 c_2} q_{\infty} z \right) \right) + O(q_{\infty}^4)$$
 (2)

The maximum value of R(0) given by (3.2.2.\$1) is confirmed by (2). It can be greater than 1. I define the phase shock width Δz by

$$[(c_1-c_2)/(1+c_1c_2)] q_{\infty} \Delta z = 2$$
(3)

Using (3.3.2.\$17) at order 1 in c_1 - c_2 :

$$\Delta z \sim 3\sqrt{2} \frac{(1+c_1c_2)(1+c_1^2)}{(c_1-c_2)^2}$$
 (4)

If moreover $|c_1|$ is small,

$$\Delta z \approx 3\sqrt{2} / (c_1 - c_2)^2 \tag{5}$$

It is now possible to specify that the solution is highly non-linear when

$$L » \Delta z(c_1, c_2)$$
 (6)

NUM 07 and NUM 06 provide a numerical example of such a case with, moreover, small c_1 - c_2 .

The **phase diffusion** equation (A3.2.\$9), governing the bulk when (6) holds, is invariant under any space translation. Therefore, the phase shock position is neutrally stable (translating the phase shock produces a steady dissymmetrical pattern). However, this neutral equilibrium is just an approximation: one neglects the (repulsive) effect of the obstacle ends on the phase shock, that is actually in the situation of a ball in a very flat potential well: when pushed away from its equilibrium position, it comes back very slowly, or does not even come back, because of solid friction. In computations, round-off errors might play the role of solid friction; in experiments, the question is unessential, because small non-uniformities are always present, and predominant. In summary, the phase shock location is practically undetermined, but this does not deny the unicity of the t-sinusoidal solution of the GLCKO model.

It is easy to check that the asymptotic solution of GLCK1 (periodic boundary conditions) is the parallel plane wave, corresponding to parallel shedding. This remark proves that the no-oscillation boundary conditions are liable for the non-uniformity of the solution of GLCK0.

3.4. The transient (starting from noise)

The transient starting from noise, described by Albarède, Provansal and Boyer (ref.), features the saturating growth of three plane wave sections: one parallel plane wave section, and two oblique plane wave sections, with opposite wave numbers, **invading** the whole interval (c.f. HT 01, HT 02, DRA 04, NUM 08, NUM 09, NUM 10, NUM 11, NUM 12, NUM 13). After the earlier "Landau" stage of the transient, $R \approx 1$ and the bulk is governed by the phase diffusion equation (A3.2.\$9). The three plane wave sections connect smoothly through two phase shocks, launched from the ends and moving inwards at speed

$$v_i = q_{\infty}(c_1 - c_2) \tag{1}$$

The eventual collision of phase shocks leads to the asymptotic t-sinusoidal state. Using the first order of (3.3.2.\$17) for q_{∞} , the transient duration is

$$L/(2v_i) \sim \frac{3\sqrt{2}}{4} \frac{1+c_1^2}{(c_1-c_1)^2} L$$
 (2)

Since the oblique wave number is obviously not affected by the collision, it is identical to that of a semi-infinite case, found in § 3.3.2., if (3.3.3.\$6) holds.

4. Experiments showing the time-sinusoidal solution of the GLC0 model

Experimental determination of the coefficients μ_p c₁ and c₂.

4.1. Near threshold experiments

Mathis, Provansal, Boyer (ref.) gave the experimental evidence of a Landau equation. Of course, their apparatus was not designed to observe the 2D flow. The amplitude modulus variation along z found by Mathis, Provansal, Boyer (ref. 2) had the sinusoidal shape of eigenfunction S_1 , meaning that the Kuramoto length of the obstacle was not much greater than π . Their Landau equation (2.2.2.\$2) was certainly not (2.2.2.\$5), but (3.3.1.\$8). Without Kuramoto rescaling, (2.3.\$1), (3.3.1.\$7) and (3.3.1.\$8) lead to a revamped version of their model:

$$v(Re, t, x = 5d, 0, z) = real(A_1(t) sin(q_1(z+L/2)) f(0)) with q_1 = \pi/L$$
 (1)

$$d_t A_1 = (\sigma_r - \mu_r q_1^2 + i(\sigma_i - \mu_i q_1^2)) A_1 - (3/4) (I_r + iI_i) |A_1|^2 A_1$$
(2)

(Actually, with the notations of § 2.2.2., $\sigma' = \sigma - \mu q_1^2$.)

The y component of f(0) is set to unity so that

$$v_y(Re, t, 5d, 0, z) = real(A_1(t) sin(q_1(z+L/2)))$$
 with $q_1 = \pi/L$ (3)

4.1.1. Determination of $\sigma_{\pmb{r}}, \mu_{\pmb{r}}$

The experimental results of Mathis, Provansal, Boyer (ref.), or Strykowski (ref.) lead to:

$$\sigma_r - \mu_r q_1^2 = k (Re - Re_1) \text{ with } k = (0.20 \pm 0.02) \text{ v/d}^2 \text{ for } Re < 60 \text{ at least}$$
 (1)

Re₁ is the critical Reynolds depending on $q_1 = \pi / L$. Identically:

$$\sigma_r = k (Re - (Re_1 - k^{-1} \mu_r q_1^2))$$

(Re₁- k^{-1} μ_r q_1^2) must be independent of L since (by dimensional analysis) $\sigma_r d^2/v$ is a function of Re only; in consequence,

$$\sigma_r = k (Re-Re_0)$$

$$Re_1 = Re_0 + k^{-1} \mu_r q_1^2$$
 (2)

With the data of Mathis (ref.), recalled on EXP 01, I check the relation (2) on EXP 02 and EXP 03. The experimental apparatus is described by Mathis (ref.), Provansal (ref.). The obstacle length remained constant (10 cm), while the

diameter varied. Resulting from EXP 02,

$$k^{-1} \mu_r = 193 d^2 \text{ or } \mu_r = 39 \text{ v}$$
 (3)

I performed an other test with constant d and variable L. From EXP 04, μ_r = 24 v. For EXP 05, each threshold was determined by extrapolating the linear relation energy-Re, and I obtain

$$\mu_r = 32 \text{ v, for Re} < 53$$
 (4)

The experiments of EXP 01 and EXP 04 differ by their EPBLs (End Plate Boundary Layer), blockage effects, etc. This may account for the discrepancy between the resulting values of μ_{Γ} I will keep the value of (4), because it is consistent with most of the experiments described hereafter. Apparently, μ_{Γ} does not depend on Re.

The Kuramoto length (c.f. § 3.2.) has a very simple expression:

$$L_K = L \sqrt{\frac{k(Re-Re_0)}{\mu_r}} = L_R \sqrt{\frac{k_R(Re-Re_0)}{\mu_{rR}}}$$

4.1.2. Determination of c2

Strykowski (ref.) found

$$c_2 = -3.0$$
 (1)

whereas a result of Provansal, Mathis, Boyer (ref.), expressed in the present context, leads to

$$|c_2| \ll k^{-1} d\sigma_i / dRe \approx 3$$
 (2)

This result is inaccurate. All other known experiments confirm Strykowski's result.

Provansal (ref. 2) monitored the evolution of energy and frequency in transients following an instantaneous shift of upstream velocity. During the transient,

$$2\pi f = \sigma_i - l_i R^2 = \sigma_i - kc_2 (Re-Re_0) R_K^2$$
, with $R_K = R/R_{sat}$ and $R_{sat}^2 = \sigma_r / l_r$ (3)

Applying this relation to the plots EXP 06, EXP 07, EXP 08 leads respectively to:

$$c_2 = -3.3, -2.8, -1.9$$

and I keep, with no bias about the dependence c2(Re),

$$c_2 = -2.7 \pm 0.7 \tag{4}$$

The negative sign of c₂ appears in 2D numerical simulations of the Navier-Stokes equations by Braza, Chassaing, Ha Minh (ref.) or Lecointe and Piquet (ref.).

For the sake of completion, I calculate the value of I_{Γ} from Mathis' data

(Mathis (ref.)). From (4.1.\$3):

$$v_y(Re, t, 5d, 0, 0) = real(A(Re, t))$$
 (5)

Cylinders with $d \le 0.7$ cm and L = 10 cm obey

$$|A| = (0.11 \pm .02) (Re-Re_1)^{1/2} v/d$$
 (6)

Consequently,

$$(0.11 \text{ V/d})^2 = (4/3) \text{ k/l}_r \tag{7}$$

$$I_r = (25\pm 8) \text{ v}^{-1}$$
 (8)

To tell the truth, the data for d > 0.8 cm give much smaller I_p , for undetermined reasons.

4.1.3. Determination of c_1-c_2

A first class of experiments allows to determine c_1 - c_2 , from the quasi-linear pulsation of mode (S_1, σ_1) , forecast by (4.1.\$2):

$$\omega_1(\text{Re}, q_1^2) = \sigma_i(\text{Re}) - \mu_i q_1^2 - c_2 (\sigma_r(\text{Re}) - \mu_r q_1^2)$$
 (1)

 c_1 - c_2 is deduced from the variation of ω_1 = $2\pi f_1$, not with Re, but the aspect ratio L_R = L/d (indeed, q_{1R}^2 = $(\pi/L_R)^2$):

$$\frac{\partial f_1}{\partial q_1^2} = -\frac{\mu_r (c_1 - c_2)}{2\pi} \tag{2}$$

From EXP 09 and (4.1.1.\$4), I get

$$\mu_{r} (c_1 - c_2) / (2\pi) = 14 v$$
 (3)

$$c_1-c_2 = 2.7$$
 at Re = 55 (4)

Energy measurements show $S_1(z)^2$.

Below $Re_m = 57$, the velocity field remains t-periodic up to more than thrice the critical length, in accordance with the GLCK0 model. At higher Re, however, a **second frequency** is possible: this point is left for § 5.1..

4.1.4. Direct measurement of c₁

An other experiment gives direct access to c_1 : I call $\omega_{1c} = 2\pi f_{1c}$ the value of ω_1 at the critical Reynolds number Re₁. The point is that this onset pulsation is **not affected** by non-linear effects, i. e. does not depend on c_2 .

$$\omega_{1c}(q_1^2) = \omega_1(Re_1(q_1^2), q_1^2) = \sigma_i(Re_1(q_1^2)) - \mu_i q_1^2$$
 (1)

Neglecting the dependence μ_i (Re), and using (1) and (4.1.1.\$2):

$$\mu_{i}/2\pi = -df_{1c}/dq_{1}^{2} + k^{-1}\mu_{r}\gamma$$
 (2)

where
$$2\pi \gamma \equiv d\sigma_i/dRe$$
 (3)

From EXP 10, df_{1c}/dq_{1}^{2} = 20.9 v. The value γ = 0.16 given by Provansal, Mathis, Boyer (ref.) cannot be used, because it is affected by the same inaccuracy as (4.1.2.\$2). I must rely on Strykowski's value (Strykowski (ref.)) to determine

 $c_1 = \mu_i / \mu_r$ and, through (4.1.3.\$4), c_2 :

$$\gamma$$
 +0.11
 c_1 -0.65
 $c_1 + 2.7 \approx c_2$ -3.35

The value of c_2 is compatible with (4.1.2.\$1) and (4.1.2.\$4).

γ can also be eliminated in the following way: I define

$$\omega_0(\text{Re}) \equiv \omega_1(\text{Re}, 0)$$
 (4)

Then, neglecting the dependence $c_2(Re)$,

$$d\omega_0/dRe = 2\pi\gamma - c_2 k \tag{5}$$

Eliminating γ from (2) and (5), I get a new access to c_1 - c_2 :

$$c_1-c_2 = 2\pi (\mu_r^{-1} df_1 c/dq_1^2 - k^{-1} df_0/dRe)$$
 (6)

 $\omega_{\mbox{\scriptsize 0}}$ is actually the plane wake pulsation. After Williamson (ref. 2),

$$df_0/dRe = Ro_1 v/d^2 = 0.2175 v/d^2$$
 (7)

The result is, again, $c_1-c_2 = 2.7$.

4.2. Far from threshold experiments

Because the Kuramoto length is much greater than π , the Landau equation (4.1.\$2) doesn't hold any longer, but a collective effect occurs: plane wave sections appear. As was first noticed by Albarède, Provansal, Boyer (ref.), the solution of the GLCK0 model, including the transient, and Williamson's experiments above $\text{Re}_{\mathbf{W}} = 64$ are qualitatively identical (apart from the existence of end cells, that is left for § 5.1.). In both cases, oblique vortex shedding originates from the boundary conditions. Williamson noticed a symmetry of the vortex field relatively to the phase shock line between the parallel shedding area (plane wave section 0) and the oblique shedding area (plane wave section 1). I call this property "symmetry law". The situation is sketched on DRA 04. A relation between x and t is introduced through a **celerity** c, simply meaning

$$v(t, x, y, z) \approx v(t-(x-5d)/c, 5d, y, z) \text{ (for } x > 5d)$$
 (1)

This relation is **not part of the GL model**. It only makes possible the exploitation of Williamson's results. The underlying problem of handling the x-coordinate and a demonstration of the symmetry law are exposed in appendix A2.

I now express the symmetry law in the context of the GLCK equation (3.1.\$3). The plane wave section 1 with wave number q has pulsation

$$\omega_{K} = c_0 - c_2 - q_{K}^2 (c_1 - c_2)$$
(2)

The plane wave section 0 with wave number zero has pulsation

$$\omega_{0K} = c_0 - c_2 \tag{3}$$

the symmetry law implies the equality of the (x, z) wave vectors (c.f. DRA 04):

$$(\omega_{0K}/c_{K})^{2} = (\omega_{K}/c_{K})^{2} + q_{K}^{2}$$
(4)

Imposing that (2) and (4) are identical for low wave numbers, I obtain

$$c_1-c_2 = (1/2) c_K^2/\omega_{0K}$$
 (5)

Introducing Kuramoto scales (3.1.\$2), ω_0 = 2π f $_0$ and c = f $_0$ λ_0 leads to

$$c_{1}-c_{2} = \frac{\lambda_{0}^{2} f_{0}}{4 \pi \mu_{r}} = \frac{\lambda_{0R}^{2} f_{0R}}{4 \pi \mu_{rR}} = \frac{\lambda_{0R}}{4 \pi \mu_{rR}} \frac{c}{V_{\infty}} Re$$
 (6)

Typically, $\lambda_{0R}\approx$ 5, μ_{rR} = 32, c/V $_{\infty}\approx$ 1 and these quantities are roughly independent of Re, giving

$$d_{Re}(c_1-c_2) \approx 10^{-2} \tag{7}$$

Therefore, (c_1, c_2) vary with Re, although this variation could be neglected without rising contradictions in § 4.1.4. $\lambda_0{}^2$ f₀, deduced from Williamson's data, is plotted on EXP 11, confirming (7). At Re = 60, $c_1{}^-c_2 \approx 340$ / $(4\pi32) \approx 0.8$, unfortunately much lower than the values of § 4.1.3. and § 4.1.4..

Williamson's parallel shedding x-wave length and angle measurements, in conjunction with the symmetry law, allow to determine the selected wave number q for each Re:

$$q = (2\pi/\lambda_0) \sin \theta \tag{8}$$

The aspect ratio is high, compared with the phase shock width: the relation (3.3.3.\$6) holds and $q_K = q_{K\infty}(c_1, c_2)$ of (3.3.2.\$17). The values of q_R and q_K resulting from experiments are plotted on EXP 18 and EXP 19 (so far, only the area Re > Re $_{\mathbf{W}}$ is concerned).

 $q_{\mbox{\scriptsize K}}$ is a function of Re only and not of the end plate radius F. The EPBL thickness δ has no effect on the wave number, whereas the GLVK0 model,

including EPBLs, predicts that q_{∞} is a function of (c_1, c_2, δ) . Paradoxically, experiments agree with the less realistic model GLCK0, where q_{∞} is a function of (c_1, c_2) , itself a function of Re. The physical explanation is that the condition A=0 is imposed at the end cell nodes, always present in Williamson's experiments (though not in GLVK0, but this is an other story). Is this node outside or inside the EPBL? At Re =150, Gerich and Eckelmann (ref.) measured the distance Δ between the node and the end plate as a function of F. At the same Re, the EPBL thickness, given by (5.1.3.\$2), is $\delta_R \approx 0.4 \; F_R^{1/2}$. Very clearly, for all values of F explored by Gerich and Eckelmann, $\Delta(F) > 2 \; \delta(F)$. The node is **outside** the EPBL, and acts as a **screen** between the wake and the EPBL! (c.f. § 2.3.). Of course, this situation should be checked for all Re.

The effect of varying (c_1, c_2) on the solution of GLCK0 is numerically inquired. The plane (c_1, c_2) is divided in two regions, as sketched on NUM 14. One of them, called the unstable region, shows non t-periodic asymptotic solutions for L high enough, and its study is left for § 5.2.. The remaining region, called the stable region, shows the (stable) chevron of § 3.3.2., with, seemingly, $q_{\infty K}$ lower than 0.55 on the stability boundary. In experiments, t-quasi-periodic and t-periodic asymptotic states are obtained respectively for Re < Re $_{\mathbf{W}}$ and Re > Re $_{\mathbf{W}}$ (forgetting end cells). Thus, $(c_1, c_2)(\text{Re} > \text{Re}_{\mathbf{W}})$ is located in the stable region and $(c_1, c_2)(\text{Re} < \text{Re}_{\mathbf{W}})$ is located in the unstable region. Moving towards the unstable region results in an increase of $q_{\infty K}$, in experiments (EXP 19) as well as in the numerical simulation of GLCK0 (NUM 23).

Remark: the parameters L_K and c_0 also depend on Re. But the variation of L_K has no effect in the stable region, as long as (3.3.3.\$6) holds, and (3.1.\$1) shows that a variation of c_0 results in a mere pulsation shift.

5. Time quasi-periodic fluctuations

5.1. The odd mode and end cells

5.1.1. Time-quasi-periodic fluctuations at short Kuramoto length

Mathis (ref.) and Mathis, Provansal, Boyer (ref. 2) observed a second mode for $Re > Re_2 > Re_1$, featuring the eigenfunction S_2 of the linearized problem (3.3.1.\$3). Moreover, EXP 13 shows that Re_2 obeys

$$Re_2 = Re_0 + k^{-1} \mu_r q_2^2, q_2 = 2\pi/L$$
 (1)

with Re₀ = 48.7 and μ_r = 42 v (instead of Re₀ = 49.7 and μ_r = 39 v determined on the first mode in identical conditions).

I carried out experiments with constant Re and variable L, revealing the approximate relation between the critical lengths

$$L_2 = 2 L_1 \tag{2}$$

(4.1.1.\$2), (1) and (2) correspond to the marginal stability conditions of modes (S_1, σ_1) and (S_2, σ_2) : real $(\sigma_n) = 0$, n = 1, 2, i.e.

$$q_n^2 = k \mu_r^{-1} (Re_n - Re_0), n = 1, 2$$
 (3)

This relation is compared with experiments on EXP 14. The agreement is not perfect, possibly because I did not use the best threshold determination method, that is extrapolating the zero of the Re-energy relation.

Coming back to the case L_R = constant, one obtains the theoretical relation:

$$Re_2-Re_0 = 4 (Re_1-Re_0)$$
 (4)

With Mathis' data, it is possible to plot Re₂ vs. Re₁, but the agreement with (4) is not very good.

The onset pulsation ω_{2c} of the second mode can be compared with the linear pulsation imag(σ_2) of mode (S_2 , σ_2). A short calculation performed at L = 2 L₁ gives:

$$\omega_1 - imag(\sigma_2) = (3/4) (c_1 - c_2) \sigma_r$$
 (5)

Two distinct experiments at Re = 68 and Re = 70 (c.f. EXP 16) give

$$\omega_{\text{1}}\text{-}\omega_{\text{2c}}<2\pi$$
 x 0.4 σ_{r} whereas

$$\omega_1$$
-imag(σ_2) = (3/4) x 2.7 x 0.2 x (70-49) = 2π x 1.4 σ_r

Is the discrepancy between ω_{2C} and imag(σ_2) a consequence of the non-linear interaction between the first mode and the second mode? GLCK0 accounts for this interaction, through (3.3.1.\$13) and (3.3.1.\$14); however, it forecasts that the

second mode is non-linearly damped by the first mode (§ 3.3.1.), and this contradicts most experiments, where $A_2 \neq 0$.

An other property of mode (S_2, σ_2) can be tried on the second mode: since the sign of S_2 changes at z=0, a node with phase opposition is expected at z=0. Gerich (ref.) published a flow visualization showing phase opposition for all x (at a given t), and gave me confirmation of phase opposition also for all t. Since $S_1(z)$ is **even** and $S_2(z)$ is **odd**, the first and second modes will be called henceforth even and odd modes. Gerich's fig. c (ref.) shows the odd mode with $L_K \approx 3.5 \pi$ (based on $\mu_T = 32 v$, $k = 0.2 \, d^2/v$, $Re_0 = 49$). The even mode is visible on fig. d, where $L_K \approx 2.2 \pi$, which is still compatible with the expected relation $L_K < 2 \pi$, allowing for a margin of error.

Numerical simulation

These experiments correspond to the quasi-linear case ($2\pi < L_K < 10$). With random noise initial conditions, mode (S_2 , σ_2) appears in GLCK0. Imposed in the initial conditions, it does grow according to the linear theory, as long as mode (S_1 , σ_1), starting from numerical noise only, is negligible. But mode (S_1 , σ_1), growing faster, eventually overwhelms and annihilates mode (S_2 , σ_2), confirming the notion of non-linear damping, and the contradiction between the GLC0 model and the existence of the odd mode.

5.1.2. Evolution of the odd mode above the threshold

I performed an experiment whith increasing L at constant Re = 70, from a subcritical length. The frequency variation appears on EXP 16, EXP 17. The global amplitude modulus of the odd mode increased quickly above its threshold, and even became greater than the global amplitude modulus of the even mode, as seen on EXP 15, where $L_K = 2.6 \pi$. Phase opposition was not checked, because only one probe was available; but the right and left frequencies (along z) were **rigorously** identical (otherwise, I would have detected a very low frequency beat). The even mode is clearly **overwhelmed** by the odd mode, as (probably) on Gerich's fig. c (Gerich (ref.)). For $L_K \approx 3\pi$, the odd mode splits apart into end cells, each remaining attached to one end of the obstacle, with slightly different frequencies f_e and f_e ' (because of a small dissymmetry). Then, the wake exhibits a strong non-linear **mixing** of three frequencies (already presented in Albarède (ref.)), with a very powerful low frequency beat at $|f_e - f_e$ '.

For higher L, the even mode regains spatial predominance in the bulk (c.f. Gerich and Eckelmann (ref.) and Williamson (ref. 2) fig. 27). The end cells are far away from each other, do not interact and are independent of L: once again, the finite length effect, through a non-linear saturation process, becomes the end effect.

5.1.3. Relation between the odd mode and the end configuration

The odd mode depends on the EPBLs

The existence of the odd mode depends on the **fetch** F, distance along which the EPBL has been growing before reaching the obstacle (fetch is the nautical term for the growth distance of wind waves, and is herein extended to a boundary layer). With F = 15 cm, L = 10 cm, d = 1.6 mm, the odd mode appears above Re₂ = 50 (Mathis (ref.)). With F = 2 cm, variable L < 7 cm, d = 1.6 mm, the odd mode appears only if Re₂ > Re_m = 57. Incidentally, this situation allows to check (3.3.1.\$11) even for $L_K > 2\pi$, provided that Re < Re_m (EXP 09). On the contrary, when Re > Re_m, the even mode frequency is strongly affected by the odd mode (EXP 17).

I checked that the EPBL thickness δ obeyed Blasius' law:

$$\delta/d \approx 5 (F/d)^{1/2} Re^{-1/2}$$
 (1)

$$\delta_{K}(Re, F) \approx 5 (kF_{R}/\mu_{r})^{1/2} ((Re-Re_{0})/Re)^{1/2} (F_{R} \text{ is F/d})$$
 (2)

 δ_K increases with Re. The EPBL may support a cell above $\text{Re}_m,$ only if δ_K exceeds a critical size.

Anyway, the flow near the ends **enhances** the odd mode: its quasi-linear limit mode $(S_2,\,\sigma_2)$ as was just shown, and, also, end cells, considered as the highly non-linear limit of the odd mode.

Breakdown of the weakly 3D approximation

The last remark suggests to introduce symmetrical EPBLs in the GL0 model, through $\sigma(\text{Re}(z))$. The resulting GLV0 model has an **even** asymptotic solution (though not necessarily t-periodic). A uniform shear on Re(z) does not produces the odd mode either.

To my mind, the odd mode **escapes** the GL0 model because the weakly 3D approximation breaks down near the ends. There, the flow is not weakly 3D, the wake is unrelated, even locally, to the plane wake, and the stability properties cannot be represented by Re(z) and GL.

5.1.4. Conclusion for § 5.1.

In quasi-linear conditions, the experimental odd mode has the threshold and shape of mode (S_2 , σ_2); in highly non-linear conditions, it takes the shape of end cells. In the GLCKO model, the odd mode is not found in the asymptotic solution, because it is non-linearly damped by the even mode.

In some experiments, the odd mode can equally be inhibited by reducing the EPBL fetch F. This shows that the odd mode is controlled and fed by the flow near the ends, a fully 3D fluid mechanics problem, that was not included in the GL model, and requires a separate study.

5.2. A theoretical explanation for Williamson's transition at $Re_W = 64$

5.2.1. Crossing the chevron stability boundary

The numerical simulation of the GLCK0 model reproduces Williamson's transition (Williamson (ref. 2)), by a slight variation of (c_1, c_2) , destabilizing the chevron. A series of numerical simulations was performed for (c_1, c_2) crossing the stability boundary. Conditions of the test: L = 48, c_0 adapted (so as to minimize $|\omega|$), c_1 variable, $c_2 = -2$, dt = 0.2, pmax = 96 (c.f. § A4.2. for information about the numerical procedure). Different stages are obtained:

- •i1: $c_1 = -0.500$ ($c_0 = -1.77$): a stable chevron.
- •i2: c_1 = -0.300 (c_0 = -1.59): a stable chevron; oscillations show up during the transient, but are eventually damped.
- •i3: $c_1 = -0.175$ ($c_0 = -1.46$): an oscillating chevron; oscillations acquire a finite amplitude (greater near the phase shock), and phase singularities (dislocations) show up during the transient.
- •i4: $c_1 = -0.120$ ($c_0 = -1.41$): a broken chevron, with two permanent internal nodes; the central cell and the lateral cells have distinct frequencies.
- •i5: $c_1 = -0.100$ ($c_0 = -1.38$): split wake. The central cell and the lateral cells are chevrons, all with the same frequency. Two neighbouring cells, separated by a node, have opposite phases (repulsive lock-in).

Each stage of the instability development (except stage i1, that is already very well known) is illustrated by the following representations:

• Lines real(A(t, z)exp(i 0.5 t)) = 0, simulating a flow visualization (HT 03, HT 04, HT 05, HT 06).

- Records $t \to R(t, z)$, standing for velocity traces (NUM 15, NUM 16, NUM 17, NUM 18).
- (q, R, ω)(z) at some given t, representative of a symmetrical asymptotic state (NUM 19, NUM 20, NUM 21, NUM 22).
- Grey tone drawing of real(A(t, z)), closer to the mathematical reality, and showing the development of phase singularities (HT 07, HT 10, HT 11, HT 12).

5.2.2. Comparison with the stability of plane waves

The linear analysis of plane wave stability was performed by Kuramoto (ref.). I recall parts of the result (where misprints have been corrected):

1• If $1 + c_1c_2 < 0$, then all plane waves are unstable, at least with respect to high wave-length perturbations.

2. In the opposite case, plane waves with

$$|q| > q_{cl} = (1 + 2(1+c_2^2)/(1+c_1^2 c_2))^{-1/2}$$
 (1)

are linearly unstable with respect to high wave-length perturbations. High wave-number plane waves, as well as high wave-number chevrons, are more likely to be unstable. For a given chevron, I call tangent plane wave the plane wave with the same wave-number. I want to compare the stability of the chevron with the stability of its tangent plane wave.

For each stage i1 to i5, I compute q_{cl} given by (1) and determine numerically the selected wave number q_{∞} . Except in stage i1, $q_{\infty} > q_{cl}$: the tangent plane wave becomes unstable between stage i.1 and stage i2. But q_{cl} is not very relevant, because it concerns the linear stability of a plane wave submitted to high wave-length perturbations, whereas I am interested in the (nonlinear) stability of a plane wave section, submitted to finite wave-length perturbations (a z-sinusoidal perturbation cannot develop if its wave-length is higher than L). Consequently, I enquire numerically the stability of plane waves (wave-number q, wave-length λ), in a periodic medium of size 2 λ (that is about the length of a chevron plane wave section, with a typical $q \approx 0.5$); stability is obtained if (and only if) $q < q_c$. The three quantities q_{∞} , q_{cl} , q_c are plotted versus c_1 on NUM 23. The result confirms that the chevron instability resembles the tangent plane wave instability, apart from (stabilizing) finite length effects.

The plane wave quasi-linear stability has not yet been investigated theoretically. But the most unstable mode seems governed by a Landau equation (the third one!), with σ_r ", I_r ". The transition (stable chevron \rightarrow oscillating chevron)

corresponds to σ_r " becoming positive, while the transition (oscillating chevron \rightarrow broken chevron) is a subcritical bifurcation, occurring when the oscillation amplitude exceeds a critical value. The temporal evolution of an unstable plane wave appears on the example HT 21: the asymptotic solution is an other plane wave (with a lower wave-number).

5.2.3. The effect of aspect ratio variation

The stable chevron is independent of the (provided high) aspect ratio; this property must be checked on the broken chevron (stage i4). By studying numerical examples, I have recognized the following scenario, valid at least for most (c_1, c_2) in the unstable region, not too far from the stability boundary, and not too far from experimental values.

In agreement with the quasi-linear stability analysis of § 3. and experiments of § 4.1., the asymptotic solution of GLCK0 is t-periodic for L small enough; consequently, a critical length $L^{(2)}(c_1,c_2)$ exists, under which the broken chevron internal nodes disappear. In the numerical examples, $L^{(2)}(c_1,c_2)$ » $\Delta z(c_1,c_2)$, so that, for L slightly lower than $L^{(2)}$, the pattern is an oscillating chevron. Using the remark of § 2.3., GLCK applies with boundary conditions taken at arbitrary nodes, in particular, the internal nodes. Therefore, for example, the distance $L^{(1)}$ between internal nodes at $L = L^{(2)}$ obeys

$$\pi \le L^{(1)}K(c_1, c_2) \le L^{(2)}K(c_1, c_2) - 2\pi$$
 (1)

When increasing L, the lateral cells keep roughly the same length $(L^{(2)}-L^{(1)})/2$. The central cell, with length L- $(L^{(2)}-L^{(1)})$, soon saturates, producing a chevron, itself unstable when its length is greater than $L^{(2)}$; a "Russian doll" cascade is started. For $N \geq 3$, I define $L^{(N)}$ as the length above which the N-th node with z > 0 appears (including the external node). I obtain, for all $N \geq 1$:

and by recurrence on N:

$$L(N)_{-L}(1) = (N-1) (L(2)_{-L}(1)) \text{ for } N \ge 1$$
(3)

If $L > \pi$, then the number of nodes (with z > 0) is simply

$$\mathcal{N}(L, c_1, c_2) = 1 + int \left(\frac{L - L^{(1)}(c_1, c_2)}{L^{(2)}(c_1, c_2) - L^{(1)}(c_1, c_2)} \right)$$
(4)

The case $(c_1, c_2) = (-0.12, -2)$ is illustrated by HT 05, HT 09, HT 11, HT 12, HT 13, HT 14, HT 15, HT 16, HT 17, HT 18, HT 19, HT 20. Some other useful results are, with $(c_0, c_1, c_2) = (-1.41, -0.12, -2)$, dt = 0.2, dz = 0.5:

$$L^{(1)}_{K} \approx 13, 33 < L^{(2)}_{K} < 36, 60 < L^{(3)}_{K} < 96, N = 6 \text{ at } L_{K} = 240$$

Practically, if L \approx L⁽³⁾, the internal nodes have an erratic motion and disappear intermittently, so that L⁽³⁾ cannot be determined precisely. The size of lateral cells is not really constant: lateral cells are dissymmetrical chevrons, evolving continuously while increasing L from a plane wave section to a symmetrical chevron. More precisely, all plane wave sections are shorter than 10 Kuramoto units, while the total length of a lateral cell is 10, 12, 16, 19 Kuramoto units for L_K = 33, 48, 60, 240. Consequently, the L^(N)'s are underestimated by (1).

But this does not deny the conclusion that a variation of L_K , as well as a variation of (c_1, c_2) , can produce a variation of N. Which process is involved in Williamson's transition must be inquired.

5.2.4. Comparison with experiments

Variable L. constant Re < Rew

Williamson did not mention that the broken chevron can be suppressed by decreasing the length, although this property seems nearly unavoidable. He did not mention either the split wake (stage i5). He only observed the broken chevron (stage i4). This was compatible with the GLCK0 model if the experiments were performed with

$$L^{(2)}K[(c_1, c_2)(Re)] < LK(Re) \cdot L^{(3)}K[(c_1, c_2)(Re)]$$
 (1)

in a neighbourhood of ${\rm Re}_{\bf W}$ (i.e. an interval]Re, Re'[containing ${\rm Re}_{\bf W}$). Williamson's range of $L_{\bf R}$ was

$$70 < L_{R} < 240$$

With Re
$$_{\rm W}$$
 = 64, μ $_{\rm r}$ = 32 ν and Re $_{\rm 0}$ = 49, $(\mu_{\rm r}/\sigma_{\rm r})^{1/2}$ = 3.27d and the range of L $_{\rm K}$ is 21 < L $_{\rm K}$ < 73

The observation of constant N = 2 below $Re_{\mathbf{W}}$ implies

$$L^{(2)}K < 21 < 73 \text{ (3)}K$$

Constant Lp. variable Re

I consider an experimental sequence where Re decreases at constant L_{R} , from above to below Re_{W} . Above Re_{W} , a stable chevron (stage i1 and stage i2) is observed. Stage i3, not easy to distinguish from the stable chevron, is not explicitly reported, although it bears a pleasant resemblance with the fig. 7 of Williamson (ref. 2): in both cases, the amplitude of oscillation is stronger near the phase shock, and the isophases of oscillation form an other chevron, pointing towards the direction opposite to that of the basic chevron! Below Re_{W} , the broken chevron (stage i4) is observed.

Williamson's transition consists in a variation of the number of nodes, caused by a variation of either L_K or (c_1, c_2) , as stated in § 5.2.3.. Let me examine the hypothesis: "in a neighbourhood of Re_w , (c_1, c_2) stays in the unstable region". It implies that the transition is caused by the variation of L_K , more precisely, the change of sign of $L_K(Re)$ - $L^{(2)}_K[(c_1, c_2)(Re)]$. The threshold should depend on L_R and, as L_K increases with Re, the broken chevron should be obtained **above** the threshold. Since those conclusions are wrong, the hypothesis is false.

Thus, $(c_1,c_2)(Re)$ moves from the unstable region to the stable region when Re increases. L_R is such as (1) holds, in a (fortunately wide) neighbourhood of Re_w. A sensitive determination of the experimental value of $(c_1,c_2)(Re_w)=(c_1w,c_2w)$ is provided by intersecting the stability boundary of NUM 14 and the straight line c_1 - c_2 = 2.7 (resulting from § 4.1.). Actually, this cannot be done accurately on NUM 14, because the intersection lies in an area where the numerical precision is poor. Therefore, I have studied the line c_1 - c_2 = 2.7 separately, with an improved precision: L = 48, c_0 adapted so as $|\omega|$ < 0.01, dt = 0.2, dz = 0.5, and I get

$$-0.55 < c_{1w} < -0.5$$
 (4)

$$-3.25 < c_{2W} < -3.2$$
 (5)

(4) and (5) are indeed not far from the results of § 4.1.4..

With $(c_0, c_1, c_2) = (-2.3, -0.45, -3.2)$, the selected wave number (obtained with π « L_K « $L^{(2)}_K$) is $q_\infty(-0.45, -3.2) = 0.57$, with a pulsation $\omega = 0.007$. Moreover,

$$30 < L^{(2)}K^{(-0.45, -3.2)} < 33$$
 (6)

and $L^{(3)}$ cannot be determined, because internal nodes move and disappear randomly. (6) disagrees with $L^{(2)}_{K} < 21$ required by (3).

6. Conclusion

6.1. Looking back

6.1.1. Solution of the GLCK0 model

The mathematical study of the solution were presented along with a non-trivial analysis of experiments, that could trouble a non-specialist reader. I give a recollection of mathematical features, without the experimental background. The result is the simplest example ever of extended system non-linear stability analysis.

The GLCK0 model consists of the GLCK equation (3.1.\$3) and no-oscillation boundary conditions. The three external parameters are c_1 , c_2 , of order unity, and L_K , length of the definition interval. The unicity and existence of a t-sinusoidal solution are proposed; it is an even function of z and therefore is called even mode.

The usual quasi-linear stability theory is applied to GLCK0: small amplitude random noise is assumed at t=0, and the time evolution is inquired. The linearized problem is diagonal in the Fourier space; the number of linearly unstable modes is $\operatorname{int}(L_K/\pi)$. For $L_K\to\pi^+$, the single linearly unstable mode is governed by a Landau equation, easily derived from GLCK.

If $2\pi < L_K « L^{(2)}_K(c_1, c_2)$, linearly unstable modes are either damped or entrained by non-linear effects, according to their parities; no distinct frequency appears, and the asymptotic solution is the even mode. If $2\pi « L_K « L^{(2)}_K$, the even mode is chevron-shaped: it is made of two symmetrical oblique plane wave sections, with wave numbers $\pm q_\infty(c_1,c_2)$ independent of L, connecting smoothly through a symmetrical steady phase shock. During the transient, after a duration of order unity, a parallel plane wave section appears, except near the boundaries, where it is replaced by oblique plane wave sections. The connection areas are phase shocks moving inwards at speed $q_\infty|c_1-c_2|$, and eventually colliding with each other at mid-span, establishing the asymptotic even mode.

Any (c_1,c_2) in the stable region yields a t-periodic asymptotic solution for all L: $L^{(2)}(c_1,c_2)=\infty$. Conversely, any (c_1,c_2) in the unstable region yields a non t-periodic asymptotic solution for some L: $L^{(2)}$ is finite (e.g. $L^{(2)}_{K}(-0.12,-2)<36$). This instability is not very different from that of the plane wave with wave number $q_{\infty}(c_1,c_2)$, and develops when q_{∞} is too high. When $L\to L^{(2)-}$, the chevron

oscillates stronger and stronger, and breaks at $L = L^{(2)}$, where, by definition, two internal nodes appear, separated by $L^{(1)}$. Between them, the central cell develops an even mode; its length increases with L, up to $L^{(2)}$, where it breaks, and so on: the same process is repeated indefinitely. The unstable region is roughly identical to, but distinct from the phase diffusion instability region, $1 + c_1c_2 < 0$.

The effect of varying (c_1,c_2) at constant L can be easily deduced from the last description: if L is greater than $L^{(2)}$ when (c_1,c_2) enters the unstable region, the transition occurs at once: the chevron splits into smaller cells. The span must be filled with as many lateral cells as possible, and the remaining length, in the range $[L^{(1)},L^{(2)}]$, is left for the central cell. In numerical examples, lateral cells are dissymmetrical chevrons, with wave-numbers q_{∞} (on most of the marginal stability boundary $q_{\infty} \approx 0.5$) and plane wave sections not exceeding a critical size. The central cell is symmetrical.

6.1.2. Experimental results

A complex amplitude A(t, z) can be associated with the experimental wake (through the definition (A1.\$5), and independently of GL). The even part of A, noted $A_T(t, z)$, is the even mode; the odd part of A, noted $A_T(t, z)$, is the odd mode; the index T recalls that $A_{\pm T}$ is invariant under $\pm T$, defined by (3.2.1.\$21). Both modes are t-sinusoidal, corresponding to t-periodic pressure-velocity fluctuations, and can be written

$$A_{\pm T}(t, z) = R_{\pm T}(z) \exp[i \int_{0}^{z} q_{\pm T}(z')dz' + i\omega_{\pm T}t]$$
 (1)

While increasing L, each mode shows

- Linear properties: growth rate, threshold, linear pulsation, shape.
- Quasi-linear properties: saturating global amplitude and pulsation, without major shape distortion.
- Highly non-linear properties: shape and pulsation have highly non-linear limits when L $\rightarrow \infty$.

The even mode

A quantitative agreement is proven between the near threshold

approximations of § 3.3.1. and experiments of § 4.1.. The even mode near the threshold is mode (S_1 , σ_1). Although not exotic, this pattern is very useful, because:

- It legitimates the GLCK0 model, in particular, the operator ∂_z^2 .
- It gives access to (c₁, c₂).

Highly non-linear properties: a qualitative agreement is obtained between, on the one hand, the far from threshold approximation of § 3.3.2., the transient of § 3.4., the instability of § 5.2., and, on the other hand, Williamson's experiments. A quantitative agreement is not reached: c_1 - c_2 is underevaluated by (4.2.\$6), q_K overevaluated on EXP 19, (5.2.4.\$3) and (5.2.4.\$6) impose contradictory conditions on $L^{(2)}_K$. But new experiments, designed on purpose, are necessary to clarify those points.

The odd mode

The GLCK0 model predicts some linear properties (threshold and shape) of the odd mode, found in experiments of § 5.1.: when $L_K \to 2\pi^+$, $A_{-T}(t,z) \sim A_2(t)$ $S_2(z)$, with a node at z=0. In most experiments, the global amplitude A_2 is clearly non-vanishing, whereas the GLCK0 model forecasts $A_2=0$.

When $L\to\infty$, A_{-T} tends towards end cells: $R_2(z)$, flattening around the central node, is negligible in the bulk. The sides of the odd mode, far from each other, are easily desynchronised by a small dissymmetry, and break apart into incoherent end cells. Again, the GLCK0 model forecasts $A_{-T}=0$.

In some experiments, however, the odd mode can be suppressed (for $Re < Re_m$) by reducing the fetch (distance between the upstream edge of the end plate and the obstacle). This property shows that the existence of the odd mode is due to the flow near the ends, that escapes the GL model, because it is not weakly 3D and cannot be approximated by a field of local plane wakes.

The fully 3D flow near a node

Near a node, the fluctuating velocity field, before going to zero, becomes fully (and awfully) 3D, and cannot be determined by the GL model; in particular, vortices from one row connect with vortices from the other row. The vorticity field obeys $\nabla . \omega(t, \mathbf{r}) = 0$, while there is no such relation for A(t, z).

Fortunately, the GLCK0 model reproduces the remote effect of external nodes, and accounts for the broken chevron. Thus, weakly 3D effects are predicted, even if the fully 3D details of the flow about the nodes are lost. One

could object that the end cell nodes do not appear in the GL0 model; the reason is probably not much the 3D complexity of this flow, but, more trivially, the fact that GL does not allow for the particular stability properties of the flow near the ends.

6.1.3. Historical conclusion (reference to other papers)

Tritton's original idea about two shedding regimes for the plane wake was wrong. Different frequencies are always the sign of a 3D cell structure, with dislocations. Gaster (ref.) had first the idea of modeling the wake by a field of coupled (Van der Pol) oscillators, but, he did not push his idea very far.

He also missed the end effect, ignored until Slaouti and Gerrard (ref.), Gerich and Eckelmann (ref.) laid emphasis on it. They promoted a new experimental attitude: before them, some parts of the problem were overshadowed, under fallacious grounds: for example, because the aspect ratio was "very high", it was taken for granted that the flow was 2D; after them, it was clear that no detail of the flow could be neglected a priori, and that the 2D schemes had to be dropped once and for all.

Van Atta and Gharib had a very high aspect ratio obstacle (L_{R} = 3500), but, as they did not investigate the 3D structure, it is difficult to conclude about their suggestion, quoted in § 1.1..

Williamson proved that substantial 3D effects remained without non-uniformities nor vibrations: they were caused by the no-oscillation boundary conditions only. This situation was very appropriate for the present purpose, because the number of mathematical external parameters was reduced to a minimum (three), while 3D effects were still non trivial.

Amplitude equations were extensively applied to closed flows, mainly convection driven by buoyancy and the rotating couette flow. Generally, internal open flows (pipe or plane Poiseuille) have subcritical transitions, that escape a description by amplitude equations. On the contrary, external open flows often have supercritical transitions. Absolutely unstable flows deserve special attention: they are governed by autonomous equations, and the instability is widely independent of the upstream noise. An other example is the hot jet, that, curiously, has about the same constant c_2 than the cylinder wake (Raghu and Monkewitz (ref.)).

The literature on wake experiments and dynamical reduction of hydrodynamical instability is so vast that I certainly miss a lot of enlightening papers (especially on the second subject).

6.2. Looking forth

6.2.1. New applications of the GL model

Other effects in a uniform flow

- Yaw: after Ramberg (ref.), yaw increases q_∞ and a transition occurs, that is qualitatively similar to the plane wave instability of HT 21.
- Forcing by vibrations (Detemple-Laacke (ref.)).
- Instability of the 2D basic flow for Re > 180: periodic boundary conditions can be used to simulate an infinite medium. GL can be modified so that the first unstable mode has a non-zero wave-number.

Non-uniform flows

The GL equation (2.3.\$2) applies to weakly 3D flows: e.g., the wake of a tapered cone (Gaster (ref. 2)), the wake of a revolution body with a periodic diameter variation d(z) (by analogy with the wake of a corrugated flat plate, studied by Meiburg and Lasheras (ref.)), etc.

Even when the GL model is a priori irrelevant, it can provide useful ideas. For example, introducing an EPBL velocity profile in GLV0 generally results in an increase of q_{∞} , and an easier release of the chevron instability. An other example is the wake of a "bi-cylinder" (a revolution body with a diameter step variation).

6.2.2. Theoretical advances

"Upstream" advances: derivation of the amplitude equation

The slow coordinates of the 3D wake are x (quasi-parallel flow) and z (weakly 3D flow). Assuming a 2D problem is equivalent to freezing the z-variation; then, the local and global stability properties are linked by an amplitude equation, with ∂_X , studied by Chomaz, Huerre, Redekopp (ref.). It should be possible as well to freeze the x-variation by assuming a parallel flow, and then link the local and global stability properties along z by an amplitude equation, with ∂_Z , indeed GL. A rigorous relationship between the complex A and the pressure-velocity field should also be derived.

Another way is to consider that the slow coordinates are x and z: the variation is slower along x and z than along y. The amplitude equation involves ∂_{x} , ∂_{z} . Rossi, Huerre, Redekopp (ref.) have studied such an equation, but I don't know if they derived it from the Navier-Stokes equations.

"Downstream" advances: solution of the GL model

The GLCK0 model deserves to be solved thoroughly: many fundamental ideas find their easiest application on this example, that is almost a mathemetical paradise, compared with other non-linear problems. The occurrence of subcritical transitions for the chevron should be confirmed. In particular, the mechanical analogy of § 3.2., and the non-linear stability analysis of plane waves should be pushed further.

There might be some interesting mathematical work on the GLVK0 model, particularly with a uniform shear on $\sigma(z)$.

6.2.3. Experimental suggestions

6.2.3.1. What experiments?

Linear stability properties

The linear stability properties of the wake are still an unexhausted mine of information, accessible through subcritical forcing or transients.

The interest of subcritical forcing is that any linear mode can be selectively excited. The drawback is that only the subcritical properties are obtained and the extrapolation of supercritical properties is hazardous.

Above the threshold, transients are obtained by turning the instability off and on, using different artifacts, such as forcing, negative feedback, base bleeding. The linear growth rate and frequency must be the same everywhere in the 3 D field (this has not yet been clearly demonstrated!).

Non-linear properties

Experiments on the even mode

- Test of (3.3.1.\$20) and (3.3.1.\$21), about the quasi-linear behaviour of q(z) and R(z). Remark: the non-linear saturation of the even mode forecast by the GLCK0 model cannot be observed if the odd mode appears ($L_K > 2\pi$).
- Direct measurement of the phase diffusion coefficient $1+c_1c_2$, by observing the relaxation of an impulse phase perturbation (at high L_K).
- The subcriticality of the transition (stable chevron \rightarrow broken chevron) could be tested by looking for hysteresis in an experiment (and a numerical simulation) where L is a slowly varying function of time (at high L_K).

Experiments on the odd mode

The fundamental question is to find why the odd mode (consisting in mode (S_2, σ_2) and end cells) appears. The evolution of the global amplitude $A_2(t)$ with Re, L, and the end plate fetch F must be inquired.

The feeding of the odd mode by the flow near the end could be represented by an forcing in the GL equation. As Slaouti and Gerrard (ref.) and Gerich and Eckelmann (ref.) found end cells with various end conditions, the feeding process seems widely independent of the details of the flow near the ends.

An other question is how and why mode (S $_2$, σ_2) splits apart into end cells (when increasing L at constant Re).

6.2.3.2. What experimental arrangement?

Two probes, one of them mobile, are necessary for phase measurements; using a row of hot wires allows simultaneous measurements at different points. LDA allows absolute non intrusive velocity measurements, but is expensive, and difficult near the end plates and the recirculating area. Base pressure measurements are also non-intrusive, and possible where LDA is not possible. Since a great number of measurements have to be performed, automatism and data-processing must be very well engineered.

Desirable features for a wind tunnel are a variable Re (30 < Re < 300), and variable end plate size and position (5 < L/d < 150 at least). Very useful are a wake instability control device and smoke visualization (that should be performed simultaneously with velocity recording). Watching obstacle vibrations is a wise precaution. For technical reasons (elastic properties, mechanical engineering), it is easier to use obstacle diameters greater than 0.2 cm. If different diameters are used, hydrodynamical similarity is not automatically respected (at least, because the size of the wind tunnel cannot be changed): it is wiser, and technically simpler, to keep a single cylinder with d = 0.2 cm. Then, the minimum z-size of the wind tunnel is 33 cm, and a suitable upstream velocity range in air is 25 cm/s < V_0 < 225 cm/s. A free stream non-uniformity of $\pm 5\%$ and turbulence level of 5% seem satisfactory.

6.2.3.3. Towards a systematic validation of the GL model

In the present work, the determination of mathematical external parameters (c_1,c_2) was partly ad hoc and I resorted to experiments performed in different

conditions and different aims; thus, building a clear picture was not easy. For any given physical external parameters L_{R} and Re, a systematic validation of GLCK0 requires:

- Determining the experimental values of σ_r , μ_r and c_0 , c_1 , c_2 (through transients or quasi-linear conditions), with an increased precision (±0.05 on c_1 and c_2).
- Solving the GLCK0 model with (L_K, c_1, c_2) deduced from experiments.
- Comparing the features of the real wake and the model solution (nodes, phase, amplitude modulus, pulsation).

6.3. About the nature and the interest of the present approach

On the one hand, a Ginzburg-Landau model is only a development of perturbation equations in powers of an external parameter near a critical value, and certainly not a physical explanation. Like all developments, it breaks down before non-analyticity. Moreover, in the present case, the validity of the GL equation is not mathematically proven, and experiments are not exhaustive.

On the other hand, the GL0 model is the first model ever to reproduce a single 3D feature of a wake. No simpler model can be proposed (otherwise non-linearity or three-dimensionality are lost), and yet, all weakly 3D features are reproduced, just by allowing for

- 1. oscillating units (local wakes);
- 2. weak three-dimensionality or weak coupling;
- 3. no-oscillation boundary conditions.

In my opinion, the fluid mechanics nature of oscillators is not involved: weakly 3D effects are organization phenomena, likely to appear in quite different situations where the last three point are encountered. As an extreme example, the chevron is a common property of a cylinder wake as well as the flight of ducks in formation (where "no-duck" boundary conditions occur!). As usual in nature, weaker interaction motion can be found with less physical knowledge. For example, the molecular structure of matter is useless to understand fluid mechanics, and, in the present case, fluid mechanics seems useless to understand weakly 3D effects in the wake of bluff bodies.

Of course, this approach breaks down when interaction is stronger: then "microscopic" properties are involved (e.g., in the present problem, the vicinity of a dislocation). Quite fortunately, however, the GL model accounts for the transition (chevron \rightarrow broken chevron).

Notes

A very interesting paper has been recently published by König, Eisenlohr and Eckelmann (ref.), concerning high aspect ratio 3D effects, but I had no time to compare it with the present work, as I did with Williamson's paper.

The experiments of Lee and Budwig (ref.), published in February 1991, are very close to those of § 4.1..

,		
	п	

A1. Definition of the complex amplitude A

The aim is **not** to derive the GL equation from the Navier-Stokes equations, but to give a link between the complex amplitude A and the pressure-velocity field, that is the only observable quantity.

The complex amplitude in the Landau model for the plane wake

The Bénard-von Kármán instability grows from those small fluctuations located in an area just downstream the obstacle, called wave maker, where the local velocity profiles are absolutely unstable. In the Landau model, the wave maker is considered as a single oscillator represented by a complex number A. Thus, the fluid oscillation at (x, y) = (5d, 0) is enough to characterize the whole wave maker.

The pressure-velocity field is $V = (p, V_x, V_y, V_z)$ (Re, t, x, y). The complex amplitude A is some complex function of Re and t such as

$$2 V(Re, t, x = 5d, y) = f(Re, A(t), y/d)$$
 (1)

The function f is then expanded in powers of A and A*:

$$f(Re, A, y) = \sum_{n} \sum_{k_1 + k_2 = n} f_{k_1, k_2} (Re, y) A^{k_1} A^{*k_2}$$
(2)

As V is real,

$$f_{k2, k1} = f_{k1, k2}^{*}$$
 (3)

 $f_{00}/2$ is the basic flow. The (non-zero) V_y component of $f_{10}(Re,\,0)$ is set to unity by convention. If A « V_∞ , it is reasonable to think that A obeys a Landau equation:

$$A_{t} = \sigma A - I|A|^{2}A \tag{4}$$

 (f_{10}, σ) is an unstable mode of the basic flow linear stability analysis. The terms of order n > 1 in (2) are responsible for non-linear effects, such as a the distortion of the time-average flow and the generation of harmonics. An observer located on the line y = 0, and sensitive to V_X only, cannot distinguish a vortex shed at y > 0 from a vortex shed at y < 0; therefore, the V_X component of $f_{10}(Re, 0)$ is zero.

The complex amplitude in the GL model for the 3D wake

Re and d may now be (slowly varying) functions of z. The pressure-velocity field is V(Re, t, x, y, z). The state of the wave maker is still represented by A, but A is allowed to vary with z:

$$2 V(t, x = 5d(z), y, z) = f(Re(z), A(t, z), y/d(z))$$
 (5)

The line (x, y, z) = (5d(z), 0, z) is taken as a representative of the whole wave maker. (The function f is the same as in the plane case.)

The GL equation is obtained by adding a diffusive coupling to the Landau equation:

$$\partial_t A = \sigma(z)A + \mu \partial_z^2 A - I(z)|A|^2 A$$
 (6)

A2. Streamwise description of the wake

The GLCK0 model describes the state of the wave maker only, that is some finite area in the streamwise direction: A(t, z) gives the shape of nascent vortices only. The downstream evolution is not simple, especially in a shear flow. However, flow visualization suggests that a simple translation rule apply in the case of uniform $V_{\infty}(z)$ and d(z): each dye filament is just translated downstream with a (phase) velocity c.

In the case of a t-periodic state, with t-period T, the translation rule is equivalent to the invariance under the translation cT in the downstream direction. This can be checked on various photographs, published by Berger (ref.), Gerrard (ref.). The rule even holds for the 3D transient appearing on fig.10 of Williamson (ref. 2). Indeed, the front velocity given by Williamson implies that the corner on a given dye filament keeps the same z while being advected; Williamson gave me confirmation of this fact.

This translation rule deserves a few remarks:

- 1. Dye filaments are somehow distorted while being advected: they develop oscillations and one corner easily gives way to two corners (Williamson (ref. 2)).
- 2. When the wake consists of many cells, the rule may apply to each cell, with its own celerity.
- 3. One should be aware that dye concentration is not the best measurement of the vorticity field: dye wraps around the vortices cores, forming filaments that subsist even if the vortices were dead. They are partly a record of the wave maker state, being translated downstream: so to speak, the visualization device acts partly as a "plotter" of the wave maker state. Thus, the translation rule may work worse for the vorticity filaments than for the dye filaments.
- 4• The translation rule is also a consequence of the experimental interest and constraints: the typical (viscous) time of evolution τ_{e} for a single vortex is greater, by a factor of order Re, than the (convective) time available for its observation τ_{o} (the time spent by the vortex within the observation section of the wind tunnel). A given vortex, once shed, has not enough time to evolve while being observed.

The unstable flow is thus approximated by a progressive wave:

$$V(t, x, y, z) \approx V(t-(x-5d)/c, 5d, y, z)$$
 (1)

Using definition (A1.\$5):

$$2 V(t, x, y, z) = f(A(t-(x-5d)/c, z), y)$$
 (2)

t is equivalent to -x/c. This property can be used to interpret graphic representations of $A(t,\,z)$ not only as the time-evolution of the wave maker, but

also as a photograph of the whole wake.

Demonstration of the symmetry law

See DRA 04.

Hypothesis: two stable semi-infinite vortex streets are connected smoothly (without dislocation), with all connection points lying in the same plane; the motion of this plane, relative to the fluid at rest, is a translation. A weak viscosity is allowed, so that the circulation κ , wave number k, and width b do not vary much in space.

The demonstration is performed in the frame of the fluid at rest. The following results are used, for a 2D stable vortex street characterized by κ , k, b:

- The pulsation ω is given by $\omega = f(\kappa, k, b)$.
- The stability is obtained when g $(\kappa, k, b) = 0$.

f and g need not be written down for the present purpose.

The streets are labeled 0 and 1. Far enough from the connection plane, each street is identical to a 2D vortex street. Each vortex 0 is connected to a vortex 1. Since circulation is the same everywhere around a vorticity pipe, $\kappa_0 = \kappa_1 \equiv \kappa$. Equating the phases of the waves 0 and 1 for all time on the translating connection plane gives $\omega_0 = \omega_1 \equiv \omega$. Thus, a set of two equations is obtained:

$$f(\kappa, k_0, b_0) = f(\kappa, k_1, b_1)$$

$$g(\kappa, k_1, b_1) = 0$$

An obvious solution for the unknown (k_1, b_1) is $(k_1, b_1) = (k_0, b_0)$. I admit that it is the only one. Thus, $(\kappa_1, k_1, b_1) = (\kappa_0, k_0, b_0)$, and the connection plane is a symmetry plane of the flow.

During the chevron transient (DRA 04, § 3.4. and Williamson (ref. 2)), the angle θ between the two waves does is steady, meaning that the connection plane is translating in the frame of the fluid at rest. The late result applies, if one neglects the influence of the obstacle on the vortex streets (correct if x > 10 d) and the direct influence of the ends.

A3. Useful results:

the Landau equation, the phase diffusion equation

A3.1. Solution of the Landau equation

$$A_{t} = (\sigma_{r} + i\sigma_{i}) A - (I_{r} + iI_{i}) |A|^{2}A$$

$$(1)$$

with $\sigma_{r} > 0, \, l_{r} > 0$ (to ensure saturation), $\sigma_{i}, \, l_{i}$ real.

Introducing $A = R \exp(i\phi)$, R > 0, in (1) leads to

$$R_t = \sigma_r R - I_r R^3 \tag{2}$$

$$\Phi_t = \sigma_i - I_i R^2 \tag{3}$$

The solution of (2) is:

$$R(t)^{-2} - I_r / \sigma_r = \exp(-2 \sigma_r t) [R(0)^{-2} - I_r / \sigma_r]$$
(4)

The asymptotic solution is sinusoidal:

$$A(t) = (\sigma_{r}/I_{r})^{1/2} \exp(i \sigma_{r} (\sigma_{i}/\sigma_{r} - I_{i}/I_{r}) t)$$
(5)

There is a non-linear shift on the pulsation.

A3.2. The phase diffusion equation

This equation was derived in a more general context by Kuramoto (ref.), for a field of coupled oscillators. Here is an elementary demonstration in the special case of the GL equation :

$$A_{t} = (1+i c_{0}) A + (1+i c_{1}) A_{zz} - (1+i c_{2}) |A|^{2} A$$
(1)

With

$$A(t, z) = R(t, z) \exp(i(c_0-c_2)t+i\Phi(t, z))$$
 (2)

the real and imaginary parts of (1) are

$$R_{t} = R - R^{3} + (R_{zz} - R\Phi_{z}^{2}) - c_{1} (2R_{z}\Phi_{z} + R\Phi_{zz})$$
(3)

$$R\Phi_{t} = c_{2}(R - R^{3}) + c_{1}(R_{zz} - R\Phi_{z}^{2}) + (2R_{z}\Phi_{z} + R\Phi_{zz})$$
(4)

After linear combinations:

$$R_{t} = R - R^{3} + (R_{zz} - R\Phi_{z}^{2}) - c_{1}(2R_{z}\Phi_{z} + R\Phi_{zz})$$
(5)

$$-c_2 R_t + R\Phi_t = (c_1 - c_2) (R_{zz} - R\Phi_z^2) + (1 + c_1 c_2) (2R_z \Phi_z + R\Phi_{zz})$$
 (6)

I study the following expansion, for some small positive $\boldsymbol{\epsilon}$:

$$R(t, z) = 1 + \varepsilon R_1(T, Z) + O(\varepsilon^2)$$
(7)

where T = ϵ t and Z = $\sqrt{\epsilon}$ z are the slow variables. Looking for Φ under the form

$$\Phi(t, z) = \Phi_0(T, Z) + O(\varepsilon)$$
(8)

(1) reduces to

$$\Phi_{0T} = -(c_1 - c_2) \Phi_{0Z}^2 + (1 + c_1 c_2) \Phi_{0ZZ}$$
(9)

$$2R_1 = -\Phi_{0Z}^2 - c_1 \Phi_{0ZZ} \tag{10}$$

In this approximation, R_1 is "slaved" by the phase Φ_0 .

A solution of (9) is

$$\Phi(T, Z) = \frac{\alpha}{\beta} \ln(\cosh(\frac{b\beta}{\alpha}(Z + 2a\beta T))) + aZ + \beta(a^2 + b^2)T$$
(11)

a and b are two real arbitrary constants,

$$\alpha = 1 + c_1 c_2, \beta = -(c_1 - c_2)$$
 (12)

For Z+2a β T \rightarrow ± ∞ , Φ represents two plane wave sections, with

$$\Phi_{Z} = a \pm b, \ \Phi_{T} = \beta (a \pm b)^{2} \tag{13}$$

The solution (11) shows the transition from a plane wave section to an other, within an area of width

$$\Delta Z = 2\alpha/(\beta b) \tag{14}$$

As ΔZ is small (before the size of the definition interval), the transition area is conventionally called a phase shock (even though it is continuous). Remarkably, β has opposite signs for chemical waves (Kuramoto (ref.)) and vortex shedding (§ 3.3.1). If α is negative, the diffusive coupling enhances instability, yielding solutions incompatible with the assumption of slow-variables. The phase diffusion equation is relevant only if:

$$\alpha > 0$$
 (15)

A4. Experimental arrangement and numerical method

A4.1. Experimental arrangement

The wind tunnel is made of a contraction supplying a 10 cm square section cylindrical pipe. In former experiments (Mathis (ref.), Provansal (ref. 1)), the end plates would be the walls of the wind tunnel: EPBLs grew along F = 15 cm (the distance between the obstacle and the pipe inlet). The obstacle length was thus L = 10 cm and different diameters d were available.

In this configuration, increasing L_R at constant Re required an upstream velocity increase, involving changes in the basic flow (e.g. the EPBLs). The blockage effect was very important for the greatest diameters (d > 0.7 cm), and not identical for all obstacles. Testing the GLCKO model was very difficult, because L_K could not be changed continuously and independently of (c_1, c_2) .

I used a different configuration, with mobile end plates and constant d =1.6 mm. The end plates were (ideally) half-planes defined by $(x \ge -F \text{ and } z = \pm \text{ L/2})$, with F = 20 mm. While moving end plates without modifying the flow input, the EPBLs, the (small) blockage effect, the local basic flows, and therefore (c_1, c_2) , remained unchanged, while L_K varied. Since cell patterns were sensitive to dissymmetry, the overall mechanical setup was preferably kept symmetrical.

At best, the turbulence level, including the measurement noise, was 5 % and the flow non-uniformity (without obstacle) was ± 5 % in the bulk. I had removed a grid at the inlet of the cylindrical pipe.

A single, mobile Laser Doppler Anemometry measurement point recorded both upstream velocity and $V_{\rm X}$ fluctuations (but not simultaneously). The obstacles were stiff aluminum rods, that could not be distorted by the air flow; they were screwed at both ends to the plexiglass walls. In a casual experiment, the rod was tied by one end only, and produced a frequency discontinuity, that disappeared when both ends were tied, meaning that the rod was allowed to oscillate due to the wall flexibility!

A4.2. Numerical method

The GL equation (2.3.\$2) is solved with

• Given complex coefficients $\sigma(z)$, $\mu(z)$, I(z). Assuming uniform coefficients does not make the numerical problem easier. Of course, accuracy is better when using Kuramoto rescaling (§ 3.1.).

- Boundary conditions: at $z \pm L/2$, either no-oscillation boundary conditions (e = 0), or periodic boundary conditions (e = 1).
- Initial conditions: when simulating a real experiment, I use random noise as initial conditions, with a turbulence level (relative random mean square) similar to that of the wind tunnel. Of ourse, in general, the choice of initial conditions is free.

A time step dt and a space step dz are chosen. I write (n, p) instead of (n dt, pdz-L/2), where n = 0, ..., nmax and p = 0, ..., pmax = int(L/dz). GL is discretized with an error $O(dt^2+dz^2)$:

$$A_t(n+1, p) = dt^{-1} 1.5 (A(n+1, p) - 2A(n, p) + 0.5 A(n-1, p)) + O(dt^2)$$
 (1)

$$A_{ZZ}(n+1, p) = dz^{-2} (A(n+1, p+1) - 2 A(n+1, p) + A(n+1, p-1)) + O(dz^2)$$
 (2)

GL is linearized using

$$|A(n+1, p)|^2 A(n+1, p) = |2A(n, p)-A(n-1, p)|^2 A(n+1, p) + O(dt^2)$$
 (3)

With

$$r(n+1, p) / dz^2 = dt^{-1} 1.5 - \sigma(p) + I(p) | 2A(n, p) - A(n-1, p) |^2 + dz^{-2} 2\mu(p)$$
 (4)

$$s(n+1, p) / dz^2 = dt^{-1} (2A(n, p) - 0.5 A(n-1, p))$$
 (5)

GL takes the form of a system of linear equations where the unknown is A(n+1, .), and the coefficients are $\mu(p)$, and r(n+1, .), s(n+1, .), functions of A(n, .), A(n-1, .):

$$-\mu(p) A(n+1, p-1) + r(n+1, p) A(n+1, p) -\mu(p) A(n+1, p+1) = s(n+1, p)$$
 (6) for $p = 1-e, ..., pmax -1$ (if $e = 1$, I consider that p is defined modulo pmax).

If e = 0, then A(n+1, 0) = A(n+1, pmax) = 0 and

$$\begin{pmatrix} r(1) & -\mu(1) & 0 & \cdots & 0 \\ -\mu(2) & r(2) & -\mu(2) & \ddots & \vdots \\ 0 & -\mu(3) & \ddots & r(pmax-2) & -\mu(pmax-2) \\ \vdots & \ddots & 0 & -\mu(pmax-1) & r(pmax-1) \end{pmatrix} \times \begin{pmatrix} A(1) & \vdots & \vdots & \vdots & \vdots \\ A(pmax-1) & \vdots & \vdots & \vdots & \vdots \\ A(pmax-1) & s(pmax-1) & s(pmax-1) \end{pmatrix}$$

If e = 1, then A(n+1, 0) = A(n+1, pmax) and

$$\begin{pmatrix} r(0) & -\mu(0) & 0 & -\mu(0) \\ -\mu(1) & r(1) & -\mu(1) & \ddots & \\ 0 & -\mu(2) & \ddots & \ddots & 0 \\ -\mu(pmax-1) & 0 & -\mu(pmax-1) & r(pmax-2) \end{pmatrix} \times \begin{pmatrix} A(0) \\ \vdots \\ \vdots \\ A(pmax-1) \end{pmatrix} = \begin{pmatrix} s(0) \\ \vdots \\ \vdots \\ s(pmax-1) \end{pmatrix}$$

With P = pmax-2+e, both cases are summarized by

$$\begin{pmatrix} r_{0} & b_{0} & 0 & eb_{0} \\ b_{1} & r_{1} & b_{1} & \ddots & \\ 0 & b_{2} & \ddots & \ddots & 0 \\ \vdots & \vdots & \vdots & \vdots & \vdots \\ eb_{P} & 0 & b_{P-2} & r_{P-1} \end{pmatrix} \times \begin{pmatrix} a_{0} \\ \vdots \\ \vdots \\ a_{P-1} \end{pmatrix} = \begin{pmatrix} s_{0} \\ \vdots \\ \vdots \\ s_{P-1} \end{pmatrix}$$

$$(7)$$

This system is solved by Gauss elimination with no pivoting, and back-substitution.

A higher time step can be used if c_0 is adapted, i.e. shifted to minimize the z-maximum modulus of the pulsation $\omega = \partial_t \arg(A(t,z))$ (c.f. § 3.1.). With c_1 , c_2 of order unity, an accurate solution requires dt < 0.5 and dz < 1. FORTRAN77 simple precision complex arithmetics was used, on a Sun 4/260 work station.

					:	
		•				

References

P.Albarède. Perturbations tridimensionnelles du sillage d'un cylindre à bas nombre de Reynolds. Stage de Magistère Interuniversitaire de Physique, Université Paris 6, juin 1989.

P.Albarède, M.Provansal, L.Boyer. Modélisation par l'équation de Ginzburg-Landau du sillage tridimensionnel d'un obstacle allongé. C. R. Acad. Sci. Paris, t. 310, Série II, p. 459-464, 1990.

E.Berger. Unterdrückung der laminaren Wirbelströmung und des Turbulenz-einsatzes der karmánischen Wirbelstrasse bei kleinen Reynoldszahlen. Jachbuch der 1964 WGLR.

E.Berger, R.Wille. Periodic flow phenomena. Annu. Rev. Fluid Mech. 1972. 4:313-340.

M.Braza, P.Chassaing, H.Ha Minh. Numerical study and physical analysis of the pressure and velocity fields in the near wake of a circular cylinder. J. Fluid Mech. (1986), vol. 165, pp. 79-130.

J.M.Chomaz P.Huerre L.G.Redekopp. Bifurcations to Local and Global Modes in Spatially Developing Flows. Phys. Rev. Lett. 6 0, 25 (1988).

P.Clavin. Selection of the chevron wave number. Private communication.

E.Detemple-Laake and H.Eckelmann. Phenomenology of Kármán vortex streets in oscillatory flow. Experiments in Fluids 7, 217-227 (1989).

P.G.Drazin and W.H.Reid. Hydrodynamic stability. Cambridge university press.

H.Eisenlohr and H.Eckelmann. Vortex splitting and its consequences in the vortex street wake of cylinders at low Reynolds number. Phys. Fluids A 1 (2), February 1989.

M.Gaster. Vortex shedding from slender cones at low Reynolds number. J. Fluid Mech. (1969), vol. 38, part 3, pp. 565-576.

M.Gaster. Vortex shedding from circular cylinders at low Reynolds number. J. Fluid Mech. (1971), vol. 46, part 4, pp. 749-756.

D.Gerich, H.Eckelmann. Influence of end plates and free ends on the shedding frequency of circular cylinders. J. FLuid Mech. (1982), vol. 122, pp. 109-121.

D.Gerich. A limiting process for the von Kármán vortex street showing the change from two- to three-dimensional flow.

J.H.Gerrard. The three-dimensional structure of the wake of a circular cylinder. J. Fluid Mech. (1966), vol. 25, part 1, pp. 143-164.

H.Haken. Synergetics, an introduction. Springer-Verlag 1978.

F.R.Hama. Three-Dimensional Vortex Pattern Behind a Circular Cylinder. Journal of the Aeronautical Sciences, 1957, vol. 24, p. 156

M.Hammache and M.Gharib. A novel method to promote parallel vortex shedding in the wake of circular cylinders. Phys. Fluids A 1 (10), October 1989.

P.Huerre, P.A.Monkewitz. Local and global instabilities in spatially developing flows. Annu. Rev. Fluid Mech. 1990. 22:473-537

G.E.Karniadakis, G.S.Triantafyllou. Frequency selection and asymptotic states in laminar wakes. J. Fluid Mech. (1989), vol. 199, pp. 441-469.

M.König, H.Eisenlohr, H.Eckelmann. The fine structure in the Strouhal-Reynolds number relationship of the laminar wake of a circular cylinder. Phys. Fluids A 2 (9), September 1990.

Y.Kuramoto. Chemical Oscillations, Waves, and Turbulence. Springer-Verlag, 1984.

H.Lamb. Hydrodynamics, sixth edition. Cambridge University Press, 1932.

Y.Lecointe, J.Piquet. On the use of several compact methods for the study of unsteady incompressible viscous flow round a circular cylinder. Computers & Fluids Vol. 12, No. 4, pp. 225-280, 1984.

T.Lee, R.Budwig. A study of the effect of aspect ratio on vortex shedding behind circular cylinders. Phys. Fluids A 3 (2), February 1991.

C.C.Lim. Dynamics of the Von Kármán vortex street. Ph.D. Brown University, 1987.

C.Mathis. Propriétés des composantes de vitesse transverses dans l'écoulement de Bénard-von Kármán aux faibles nombres de Reynolds. Thèse, Université de Provence, 1983.

C.Mathis, M.Provansal and L.Boyer. The Bénard-von Kármán instability: an experimental study near the threshold. J. Physique Lett. **4 5** (1984) L-483 - L-491.

C.Mathis, M.Provansal, L.Boyer. The rotating grating applied to the study of the Bénard-von Kármán instability near the threshold. Proc. Second Intl. Symp. on Applications of Laser Anemometry to Fluid Mechanics, Lisbon, 1984.

E.Meiburg and J.C.Lasheras. Experimental and numerical investigation of the three-dimensional transition in plane wakes. J. Fluid Mech. (1988), vol. 190, pp.1-37.

P.A.Monkewitz. The absolute and convective nature of instability in two-dimensional wakes at low Reynolds number. Phys. Fluids 3 1 (5), May 1988.

P.A.Monkewitz. Near threshold expansion of the GLCK0 model t-sinusosidal solution. Private communication.

M.Provansal. Etude expérimentale de l'instabilité de Bénard-von Kármán.Thèse, Université de Provence, 1988.

M.Provansal. Energy-frequency measurements during transients. Private communication.

M.Provansal, C.Mathis, L.Boyer. Bénard-von Kármán instability: transient and forced regimes. J. Fluid Mech. (1987), vol. 182, pp. 1-22.

S.Raghu, P.A.Monkewitz. The bifurcation of a hot round jet to limit-cycle oscillations. To be published in Physics of Fluids A.

S.E.Ramberg. The effects of yaw and finite length upon the vortex wakes of stationary and vibrating circular cylinders. J.Fluid Mech. (1983), vol. 128, pp. 81-107.

M.Rossi, P.Huerre, L.G.Redekopp. A model of Boundary Effects in Kármán Vortex Streets. Bulletin of the American Physical Society. Vol. 34, No. 10 (1989).

J.Y. Sa, K.S. Chang. Shedding patterns of the near-wake vortices behind a circular cylinder. To be published in Int. J. for Numerical Methods in Fluids.

A.Slaouti, J.H.Gerrard. An experimental investigation of the end effects on the wake of a circular cylinder towed through water at low Reynolds numbers. J. Fluid Mech. (1981), vol. 112, pp. 297-314.

K.R.Sreenivasan, 1985 Transition and turbulence in fluid flows and low-dimensional chaos. In *Frontiers in Fluid Mechanics* (ed. S.H.Davis & J.L.Lumley), pp. 41-67. Springer.

P.J.Strykowski. The control of absolutely and convectively unstable flows. Ph. D. Yale University, 1986.

G.S.Triantafyllou, G.E.Karniadakis. Computational reducibility of unsteady viscous flows. Phys. Fluids A 2 (5), May 1990.

D.J.Tritton. Experiments on the flow past a circular cylinder at low Reynolds numbers. J. of Fluid Mech. (1959) vol. 6, pp.547-567.

D.J.Tritton. A note on vortex streets behind circular cylinders at low Reynolds numbers. J. of Fluid Mech. (1971) vol. 45, part 1, pp. 203-208.

C.H.K.Williamson. The existence of two stages in the transition to three-dimensionality of a cylinder wake. Phys. Fluids 3 1 (11), 3165, November 1988.

C.H.K.Williamson. Oblique and parallel modes of vortex shedding in the wake of a circular cylinder at low Reynolds numbers. J. FLuid Mech. (1989), vol. 206, pp. 579-627.

Bibliography

E.Berger. Suppression of Vortex Shedding and Turbulence behind Oscillating Cylinders. The physics of fluids supplement, 1967.

D.Gerich. The development of three dimensionality in the near and in the far wake due to changes of the boundary conditions. Tenth Australasian fluid mech. conference. Univ. of Melbourne, 11-15 December 1989, vol. 2.

J.H.Gerrard. The wakes of cylindrical bluff bodies at low Reynolds number. Phil. Trans. Roy. Soc. London A, <u>288</u>, p.351 (1978).

L.S.G.Kovásznay. Hot-wire investigation of the wake behind cylinders at low Reynolds numbers. Proc. R. Soc. A 198 (1949) 174.

D.Lazimi. The flame of genius at low Markstein numbers. The Dead Sea Phil. Soc. Jerusalem. Special issue, January 1991.

H.Oertel Jr., Wakes behind blunt bodies, Annu. Rev. Fluid Mech. 1990, 22: 539-64.

A.Roshko. NACA technical note 2913. On the development of turbulent wakes from vortex streets. March 1953.

J.W.Schaefer, S.Eskinazy. An analysis of the vortex street generated in viscous fluid. J. Fluid Mech. (1959), vol. 6, pp. 241-260.

S.Taneda, Rep. Res. Inst. Appl. Mech. 1, 131(1952).

C.H.K.Williamson. The development of Λ -shaped vortical structures caused by "vortex dislocations" in a planar wake. Phys. Fluids A, Vol. 1, No. 9, September 1989, Gallery of Fluid Motion.

		,

Abstract

The wake of an elongated bluff body at low Reynolds numbers is considered as a chain of coupled oscillators, obeying a Ginzburg-Landau equation, with no-oscillation boundary conditions.

The problem is solved, either numerically, either analytically. Analogies are provided with a quantum well, with a (non-hamiltonian) point mechanics problem. The interactive comparison between the model and experiments shows the following points:

- ·Boundary conditions do play a major role.
- •To some extent, varying the Reynolds number or the aspect ratio have identical effects.
- Near the threshold, a quasi-linear description is legitimate.
- •Far from the threshold, a chevron-shaped pattern appears and may be unstable.

The Ginzburg-Landau model, in spite of its maximal simplicity, accounts for most experimental space-time effects. It solves plenty of contradictions, and pioneers a new way to understand the instability of three-dimensional wakes.

Key words

Open flow, wake, Bénard-von Kármán instability, absolute instability, 3D vortex field, Ginzburg-Landau equation, chevron, wave-number selection, phase diffusion, self-organization, phase singularities.